OPEN

Evaluation of Physicochemical Properties, Pharmacokinetics, Biodistribution, Toxicity, and Contrast-Enhanced Cancer MRI of a Cancer-Targeting Contrast Agent, MT218

Yajuan Li, PhD, Songqi Gao, PhD,* Hongfa Jiang, MSc,* Nadia Ayat, PhD,† Victoria Laney, MSc,† Calin Nicolescu, BSc,† Wenyu Sun, MD,† Michael F. Tweedle, PhD,‡ and Zheng-Rong Lu, PhD†§*

Objectives: Preclinical assessments were performed according to the US Food and Drug Administration guidelines to determine the physicochemical properties, pharmacokinetics, clearance, safety, and tumor-specific magnetic resonance (MR) imaging of MT218, a peptidic gadolinium-based MR imaging agent targeting to extradomain B fibronectin for MR molecular imaging of aggressive tumors.

Materials and Methods: Relaxivity, chelation stability, binding affinity, safety-related target profiling, and effects on CYP450 enzymes and transporters were evaluated in vitro. Magnetic resonance imaging was performed with rats bearing prostate cancer xenografts, immunocompetent mice bearing murine pancreatic cancer allografts, and mice bearing lung cancer xenografts at different doses of MT218. Pharmacological effects on cardiovascular, respiratory, and central nervous systems were determined in rats and conscious beagle dogs. Pharmacokinetics were tested in rats and dogs. Biodistribution and excretion were studied in rats. Single and repeated dosing toxicity was evaluated in rats and dogs. In vitro and in vivo genotoxicity, in vitro hemolysis, and anaphylactic reactivity were also performed.

Results: At 1.4 T, the r_1 and r_2 relaxivities of MT218 were 5.43 and 7.40 mM^{-1} s^{-1} in pure water, 6.58 and 8.87 mM^{-1} s^{-1} in phosphate-buffered saline, and 6.54 and 8.70 mM^{-1} s^{-1} in aqueous solution of human serum albumin, respectively. The binding affinity of MT218 to extradomain B fragment is 3.45 μM. MT218 exhibited no dissociation of the Gd(III) chelates under physiological conditions. The peptide degradation half-life ($t_{1/2}$) of MT218 was 1.63, 5.85, and 2.63 hours in rat, dog, and human plasma, respectively. It had little effect on CYP450 enzymes and transporters. MT218 produced up to 7-fold increase of contrast-to-noise ratios in the extradomain B fibronectin–rich tumors with a dose of 0.04 mmol/kg for at least 30 minutes. MT218 had little pharmacological effect on central nervous, cardiovascular, or respiratory systems. MT218 had a mean plasma elimination half-life ($t_{1/2}$) of 0.31 and 0.89 hours in rats and dogs at 0.1 mmol/kg, respectively. No detectable Gd deposition was observed in the brain at 6 hours postinjection of MT218 at 0.1 mmol/kg in rats. MT218 was not mutagenic and had no mortality or morbidity in the rats or dogs up to 1.39 and 0.70 mmol/kg/d, respectively. The no observed adverse effect level of MT218 in Sprague-Dawley rats was 1.39 mmol/kg for single dosing and 0.46 mmol/kg/d for repeated dosing. The no observed adverse effect level in dogs was 0.07 mmol/kg/d. MT218 exhibited no genotoxicity, hemolysis, and anaphylactic reactivity.

Conclusion: The preclinical assessments showed that the targeted contrast agent MT218 has high r_1 and r_2 relaxivities, satisfactory physicochemical properties, pharmacokinetic, and safety profiles and produces effective tumor enhancement in multiple cancer types in rats and mice at reduced doses.

Key Words: ZD2-N_3-(Gd-HP-DO3A), extradomain B fibronectin, cancer-specific, magnetic resonance imaging, contrast agent, pharmacokinetics, toxicology

(*Invest Radiol* 2022;57: 639–654)

The Gd(III)-based contrast agents (GBCAs) commonly used in contrast-enhanced magnetic resonance imaging (MRI) pass through compromised blood-brain barriers, preferentially accumulating in and enhancing T_1 MRI signal in growing brain tumors.[1] The lack of a blood-tissue barrier in non–central nervous system (CNS) tissue has made the use of GBCA in the body more challenging. Dynamic contrast-enhanced MRI with GBCAs takes advantage of differences in tumor and tissue vascular permeability to characterize tumors in the body.[2] It is thus an important component of multiparametric MRI (mpMRI) for diagnostic imaging and surgery planning of prostate cancer.[3,4] Despite some specific clinical successes, multiparametric MRI and other GBCA-based MRI detection methods are the exception in the body owing to the lack of tumor specificity of the GBCA. There is thus an unmet need for targeted MRI contrast agents for accurate high-resolution detection and characterization of aggressive tumors to guide efficacious treatment at the earliest possible stage to improve the survival of cancer patients. An innovative design of a targeted MRI contrast agent specific to a cancer biomarker would have a significant impact to advance magnetic resonance molecular imaging (MRMI) for precision cancer imaging.

There have been continuous efforts to design and develop targeted MRI contrast agents since the clinical application of MRI in the early 1980s.[5–9] Antibody targeted GBCAs were explored to target the biomarkers on cancer cell surfaces. Because of the low concentration of the cell-surface tumor markers (typically nM) and poor sensitivity of MRI for molecular imaging GBCA (typically μM), these targeted contrast agents have been unable to generate tumor-specific MRI detectable signal enhancement.[5] Incorporation of tumor-specific antibodies and peptides into nanoparticles loaded with GBCAs deliver a sufficient amount of the contrast agents in solid tumors and produces robust signal enhancement for effective MRMI of cancer in animal tumor models.[10] However, the large size of these agents impedes rapid target accumulation and clearance of GBCAs demanded of clinically safe and useful agents.[11] Therefore, despite the efficacy of the targeted GBCA-nanoparticles in animal tumor models, they have not advanced to clinical development.

We have recently hypothesized that the design and development of small molecular targeted GBCAs specific to abundant oncoproteins in tumor extracellular matrix (ECM) would overcome the current limitations of MRI for cancer molecular imaging and precision cancer diagnosis.[12] Tumors have a unique microenvironment enriched with oncogenic ECM proteins, not present in normal tissues. Among various

Received for publication February 1, 2022; and accepted for publication, after revision, March 12, 2022.

From the *Molecular Theranostics, LLC, Cleveland; †Department of Biomedical Engineering, Case Western Reserve University, Cleveland; ‡Wright Center of Innovation, Department of Radiology, the Ohio State University, Columbus; and §Case Comprehensive Cancer Center, Case Western Reserve University, Cleveland, OH.

Conflicts of interest and sources of funding: YL, SQ, MFT, and ZRL have ownership interest in Molecular Theranostics, LLC. The work is supported in part by National Institutes of Health grants R44 CA199826 and R01 CA211762, and Jiansu Ronghui Motek Pharmaceuticals, Inc.

Correspondence to: Zheng-Rong Lu, PhD, Department of Biomedical Engineering, Case Western Reserve University, Wickenden 427, 10900 Euclid Avenue, Cleveland, OH 44106. E-mail: zxl125@case.edu; Yajuan Li, PhD, Molecular Theranostics, LLC Cleveland, OH 44114. E-mail: yli@mtheranostics.com.

ISSN: 0020-9996/22/5710–0639
DOI: 10.1097/RLI.0000000000000881

ECM proteins in tumor tissues, extradomain B fibronectin (EDB-FN) is a promising target for designing clinically translatable targeted GBCA.[13] Extradomain B fibronectin is an oncofetal isoform of FN and is highly expressed in the ECM of aggressive tumors.[14] It is considered a marker of epithelial to mesenchymal transition which is a biological program associated with invasion, metastasis, and drug resistance of multiple malignancies.[15–18] Elevated expression of EDB-FN is associated with epithelial to mesenchymal transition induction, cancer cell invasion, and metastasis.[16] It is overexpressed in various aggressive human cancers and absent in normal tissues.[19–21] Extradomain B fibronectin has been explored as an oncotarget for developing molecular imaging technologies and targeted therapeutics for cancer diagnosis and therapy. For example, antibody fragment L19 specific to EDB-FN has been used to develop positron emission tomography probes and targeted therapeutics for cancer imaging and therapy in both preclinical and clinical studies.[22] A nanobody has been developed to target EDB-FN for effective positron emission tomography imaging of different types of cancer in animal tumor models.[23] An aptamer-like peptide has also been developed to target EDB-FN to deliver imaging agents and therapeutics for cancer imaging and therapy.[24]

To encourage clinically and industrially acceptable properties, we used phage display against EDB fragment to develop a small peptide named ZD2 (Thr-Val-Arg-Thr-Ser-Ala-Asp) that has a moderate binding affinity to the EDB fragment.[25] The peptide was conjugated to a clinical contrast agent gadoteridol (Gd(HP-DO3A) or ProHance) making ZD2-Gd(HP-DO3A) with a $(CH_2CH_2O)_2$ spacer.[25] The agent was effective for MRMI of aggressive tumor detection and characterization of aggressive prostate cancer and metastatic breast cancer in mouse models.[26,27] The structure of the targeted contrast agent was further optimized to identify a lead targeted contrast agent ZD2-N_3-Gd(HP-DO3A) (MT218, molecular weight of 1442.62 Da; Fig. 1) with an improved r_1 relaxivity and a straightforward synthetic procedure for clinical translation.[28] MT218 produces robust specific magnetic resonance (MR) contrast enhancement at doses lower than those of the base GBCA in several types of aggressive tumors, including breast cancer, colorectal cancer, head and neck cancer, pancreatic cancer, and prostate cancer.[17,28–31] The enhancement pattern closely reflects relative EDB-FN expression levels in these tissue types, which is known to reflect tumor aggressiveness. MT218 in MRMI therefore has the potential for characterizing the invasiveness of solid tumor and assessing tumor response to therapies as well as development of drug resistance.[17,32] MT218 is also a small, water soluble peptidic monomer with practical industrialization potential and rapid animal pharmacokinetics as required for commercial contrast agents.

In this work, we further investigated the dosing effect of MT218 for MRI of prostate cancer xenografts in rats and its potential for detection of lung cancer and pancreatic cancer models at a low dose in mice. We also performed a comprehensive in vitro characterization and in vivo pharmacokinetics, biodistribution, and safety assessment of MT218 according to the Food and Drug Administration (FDA) guidelines for preclinical development (https://www.fda.gov/regulatory-information/search-fda-guidance-documents/developing-medical-imaging-drug-and-biological-products-part-1-conducting-safety-assessments).

MATERIALS AND METHODS

The MT218 active pharmaceutical ingredient (API) and MT218 injection were supplied by Jiangsu Ronghui Motek Pharmaceuticals, Inc (China). 1,4,7,10-Tetraazacyclododecane-1,4,7,10-tetraacetic acid (DOTA) and diethylenetriaminepentaacetic acid (DTPA) were purchased from Strem Chemicals. 10-(2-Hydroxypropyl)-1,4,7,10-Tetraazacyclododecane-1,4,7-triacetic acid (HP-DO3A) was purchased from USP (Maryland). Human, rat, and dog plasma was obtained from Equitech-Bio, Inc (Kerrville, TX). Gadoteridol (ProHance, Ga(HP-DO3A)) was purchased from Bracco Diagnostics (Monroe Township, NJ). The pooled cryopreserved human primary hepatocytes, the CD1 mouse primary hepatocytes, the Sprague-Dawley (SD) rat primary hepatocytes, and the beagle dog primary hepatocytes were supplied by BIOIVT (Westbury, NY). The pooled human liver microsomes were purchased from BIOIVT. Recombinant HEK293 cell lines stably expressing human transporters (OATP1B1, OATP1B3, OAT1, OAT3, OCT2, MATE1, and MATE2K), HEK293-MOCK cell line transfected with empty vector, human multidrug resistance protein 1 (MDR1) vesicles, and breast cancer resistance protein (BCRP) vesicles were supplied by GenoMembrane (Kanagawa, Japan). Human embryonic kidney cell line HEK-293 with stable expression of human ether-a-go-go related gene (hERG) was supplied by the Academy of Military Medical Sciences, China. Liver S9 microsomal fractions (S9) were provided by CHI Scientific (Mississippi). Histidine-deficient *Salmonella typhimurium*, TA97a, TA98, TA100, TA1535, and TA102, were obtained from Moltox (Boone, NC). Chinese hamster lung (CHL) fibroblast was obtained from Shanghai Institutes for Biological Sciences, Chinese Academy of Sciences (Shanghai, China). Procedures carried out on the animals involved in the imaging experiments were performed according to an approved protocol by the Institutional Animal Care and Use Committee (IACUC) of Case Western Reserve University. All other animal studies were performed at Joinn Laboratories (Beijing, China) following the standard operating procedures and protocols approved by the IACUC and current Good Laboratory Practice (cGLP)/non-GLP guidelines of Joinn Laboratories.

Chelation Stability

At pH 5 and 7.4, 0.25 mM MT218 was incubated with the same concentration of DOTA, DTPA, HP-DO3A, ethylenediaminetetraacetic acid (EDTA), or 0.50 mM zinc chloride and at room temperature or 37.5°C over a period of 30 days. Acetate buffer (0.05 M, pH 5) and Tris buffer (0.05 M, pH 7.4) were used to maintain the pH. A high-performance liquid chromatography–ultraviolet method (Agilent 2200, Waters Symmetry C18 column, 4.6 × 150 mm, 5 μm, mobile phase 0.08% trifluoroacetic acid acetonitrile/water) was used to analyze the remaining MT218 in the solution.

Relaxivity

Solutions of MT218 were prepared at concentrations of 0.125, 0.25, 0.5, 1, and 2 mM in human serum albumin aqueous solution (40 mg/mL), water, and phosphate-buffered saline (PBS). The T_1 and T_2 values of the MT218 solutions were measured at 1.4 T using

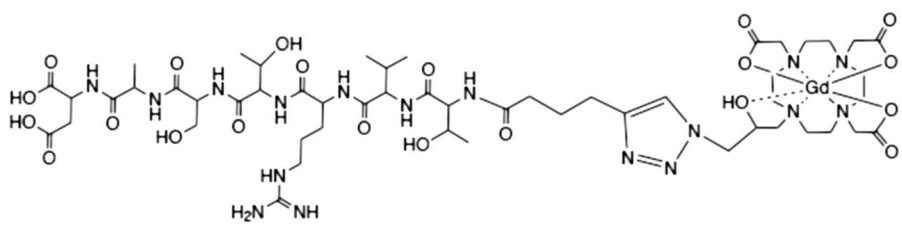

FIGURE 1. Chemical structure of the targeted MRI contrast agent MT218.

a Bruker Minispec Relaxometer (60 Hz, 37°C). The respective T_1 and T_2 values of MT218 solutions were also determined at 3 T using a 3 T MRS 3000 scanner (MR Solutions, Surrey, UK). T_1 values were measured using an inversion recovery–fast low angle shot sequence from MR Solutions. T_2 values were obtained using a multiecho multislice sequence from MR Solutions. The following equation is used to calculate relaxivities (r_1, r_2): $1/T_i = 1/T_{i,0} + r_iC$, where T_i is the observed relaxation time in the presence of the contrast agent, $T_{i,0}$ is the relaxation time of pure water, and C is the concentration of the MRI contrast agent. The subscripts indicate longitudinal ($i = 1$) or transverse ($i = 2$) relaxivities and relaxation times, respectively. The r_1 and r_2 relaxivities were calculated from the slopes of $1/T_1$ and $1/T_2$ versus MT218 concentration plots, respectively.

Binding Affinity Study

Plasmid DNA encoding EDB fragment was constructed with a T7 promoter and a decameric His-tag at the N-terminal. A Lac operon (lacO) was also incorporated to control EDB expression with Isopropyl β-d-1-thiogalactopyranoside (IPTG) induction. The recombinant EDB expressing plasmid was transformed into *Escherichia coli* strain BL21 (DE3)-T1, and EDB expression was induced by the addition of 1 mM IPTG at the midlog phase of bacterial growth and incubated for 3 hours. The bacteria were collected and lysed with lysozyme. Extradomain B was purified using a HisTalon SuperFlow cartridge and lyophilization. The size and purity of the extracted EDB protein were determined by sodium dodecyl sulfate-polyacrylamide gel electrophoresis. Extradomain B protein protein fragment (5 mg/mL) was further purified with a PD-10 desalting column using pH 7.4 10 mM PBS buffer as the mobile phase.

The binding affinity of MT218 to EDB protein fragment was determined using surface plasmon resonance. Stock solution of MT218 (1.0 mM) was prepared with a running buffer (0.05% Tween-20 in 10 mM PBS, pH 7.4). The active and reference flow cells of a CM5 sensor chip (Cytiva, Sweden) were activated with amine coupling kit, and EDB protein (25 μg/mL) in 10 mM acetate buffer (pH 4.5) was injected into the active cell for 3 minutes at a rate of 10 μL/min to immobilize the protein at a level of 1500 RU. Then both the reference and flow cells were blocked with ethanolamine (pH 8.5) for 7 minutes. The system was then switched to running buffer, and varying concentrations of MT218 were injected for 120 seconds at 50 μL/min, with 5 minutes of dissociation. Binding affinity was determined using Biocore T200 Evaluation Software 3.1. Microsoft Office Excel (2019) was used for statistical analysis of data, including mean, standard deviation, and coefficient of variation (CV %).

Plasma Protein Binding

Nonspecific binding of MT218 to plasma proteins was determined by incubating with human serum albumin (40 mg/mL), human, dog, rat plasma, and PBS at 37°C for 3 minutes at concentrations of 50, 80, and 110 μM, respectively. After incubation, MT218 (or gadolinium [Gd]-containing degradants) was separated by centrifugation using a 10 kDa cut-off filter at the speed of 14,000*g* at 4°C for 30 minutes. Filtrate (300 μL) from each sample tube was transfered to a 15-ml metal free Eppendorf tube, and 9.7 ml of 3% nitric acid was then added. The mixture was kept overnight. Then the samples were centrifuged to remove insolubles and tested by inductively coupled plasma-optical emission spectrometry (ICP-OES 730, Agilent, Santa Clara, CA after agilent) for Gd content. The total MT218 binding to plasma proteins was calculated into the binding ratio.

Plasma Stability

MT218 (0.5 mM) was incubated in human, rat, and dog plasma at 37°C for 48 hours. Phosphate-buffered saline was used as control. The mixture was mixed with methanol, followed by centrifugation, and then measured using analytic high-performance liquid chromatography (Agilent 1260 Infinity DAD LC, column Phenomenex C18, 4.6 × 250 mm, 5 μm; phase A: 0.08% TFA·H_2O; phase B: 0.08% trifluoroacetic acid in acetonitrile; 0–13 minutes phase B, 0%–13%). The percentage ratio of remaining MT218 was calculated.

Metabolism

In a series of non-GLP studies, metabolic stability, metabolite identification, and possible metabolic pathway of MT218 were investigated by incubation with hepatocytes from human, CD1 mouse, SD rat, beagle dog, and cynomolgus monkey following FDA guidance on in vitro drug interaction studies. Testosterone and midazolam (substrates of CYP3A4) and 7-hydroxycoumarin (substrate of uridine 5′-diphospho-glucuronosyltransferase) were used as positive controls. The inhibition effect of MT218 on main members of cytochrome P450 (CYP450) family, including CYP1A2, CYP2B6, CYP2C9, CYP2C19, CYP2D6, and CYP3A4, was evaluated using pooled human liver microsomes at the MT218 concentration from 0.01 to 100 μM. The final concentration of the human liver microsomes was 0.5 mg/mL. The induction potential on CYP1A2, CYP2B6, and CYP3A4 was also investigated using omeprazole (50 μM), phenobarbital (1000 μM), and rifampicin (25 μM) as positive control. The potential inhibition of MT218 on solute carrier family transporters MDR1, BCRP, organic anion transporting polypeptides (OATP1B1, OATP1B3), organic anion transporters (OAT1, OAT3), organic cation transporter 2 (OCT2), and multidrug and toxin extrusion proteins (MATE1 and MATE2K) was evaluated. The inhibition potential of MT218 on human MDR1 and BCRP was assessed using membrane vesicles expressing MDR1 and BCRP, respectively, according to the FDA's guidance (https://www.fda.gov/regulatory-information/search-fda-guidance-documents/vitro-drug-interaction-studies-cytochrome-p450-enzyme-and-transporter-mediated-drug-interactions). For all the other transporters, HEK293 cells expressing these transporter proteins were used. Cyclosporine A (20 μM), novobiocin (100 μM), rifampin (100 μM), quinidine (500 μM), probenecid (50 μM), and pyrimethamine (10 μM) were used as inhibitors, respectively. The MT218 concentrations were 100, 50, 10, 5, and 1 μM. The samples were analyzed using the Shimadzu LC20 liquid chromatography (Shimadzu Co, Ltd, Japan) system and API 4000 triple-quadrupole mass spectrometer (Applied Biosystems Inc).

Cell Culture

LNCaP and PC3 human prostate cancer cell lines and H1299 human lung cancer cell line were purchased from ATCC (Manassas, VA). The cell lines were cultured in RPMI 1640 medium (Gibco, Waltham, MA) supplemented with 10% fetal bovine serum and 100 units/mL penicillin/streptomycin. All the cells were grown at 37°C and 5% CO_2. KPC-K8484 (herein KPC) cells were generously provided by the lab of Dr Jordan Winter (University Hospitals of Cleveland and CWRU, Cleveland, OH). KPC cells were maintained in RPMI 1640 Medium supplemented with 10% fetal bovine serum (Sigma-Aldrich, St Louis, MO) and 1% penicillin/streptomycin (Thermo Fisher Scientific, Waltham, MA).

Western Blot

Total protein was extracted from cancer cells as previously described.[16] Protein concentration was determined by Lowry assay. Equal amounts of protein extracts (40 μg) were loaded onto sodium dodecyl sulfate-polyacrylamide gel electrophoresis for electrophoresis and transferred onto nitrocellulose membranes. The following primary antibodies (1:1000 dilution, overnight incubation at 4°C) were used: anti-β-Actin (Cell Signaling Technology, Danvers, MA) and anti-EDB-FN (G4 clone, Absolute Antibody, UK). Following secondary antibody incubation (1:2000 dilution for 2 hours), the membranes were developed using Signal Fire Plus ECL Kit (Cell Signaling Technology) and imaged on ChemiDoc XRS+ Imager (Bio-Rad, Hercules, CA).

Rat Tumor Xenograft Mouse Models

Adult male NIH-*Foxn1*^{rnu} nude rats were obtained from Charles River Laboratories (Wilmington, MA). The rats were housed in the Animal Facility at CWRU and all animal experiments were performed according to the protocols approved by IACUC. The lateral flanks of 10 rats were subcutaneously injected with either 4×10^6 PC3 or 8×10^6 LNCaP cells suspended in a Matrigel-PBS mixture (1:1). Once the tumor volume exceeded 100 mm^3, rats were subjected to MRI. A total of 20 male rats were used to develop subcutaneous xenografts of human prostate cancer. Ten rats were subcutaneously implanted with either PC3 or LNCaP human prostate cancer cells. Six rats developed visible PC3 tumors within 5 weeks and only 3 rats developed LNCaP tumors within 6 weeks.

Mouse Tumor Xenograft Mouse Models

For the protein kinase C (PKC) pancreatic cancer model, C57BL/J6 immunocompetent mice (6-week-old males and females) were purchased from the Jackson Laboratory (Bar Harbor, MA). KPC-K8484 cells (1×10^5) suspended in Matrigel-PBS mixture (1:1) were subcutaneously injected into the left flank of the B6 mice (100 μL per mouse, 5 mice per group). Magnetic resonance molecular imaging with MT218 was performed at 1 and 5 weeks after tumor inoculation. For lung cancer model, nude athymic mice (6-week-old nu/nu males) were purchased from Jackson Laboratory. About 5–6 $\times 10^6$ H1299 cells suspended in Matrigel-PBS mixture (1:1) were subcutaneously injected in the left flanks of the mice. The mice were housed and cared in the Animal Facility at CWRU.

MRI With MT218

Magnetic resonance imaging was performed on a 3 T MRS 3000 scanner (MR Solutions) with a mouse short quad coil or a rat short quad coil (MR Solutions) with respiratory gating. The animals were anesthetized with isofluorane and tail vein catheter was setup. For mouse MRI, T_1-weighted MR images were obtained before and after injection of MT218 at a pre-determined dose with axial fast spin echo sequence (repetition time, 305 milliseconds; echo time, 11 milliseconds; flip angle, 90 degrees; field of view, 40 mm × 40 mm; slice thickness, 1 mm; slice number = 15; number of average, 2; matrix, 256 × 256). For rat MRI, T_1-weighted images were acquired before and after injection of MT218 at doses of 0.04 or 0.02 mmol/kg, using a fast spin-echo sequence with respiratory gating (repetition time, 305 milliseconds; echo time, 11 milliseconds; field of view, 80 × 80 mm; slice thickness, 1 mm; number of average, 2; matrix, 128 × 128). The imaging protocol was repeated with the clinical agent ProHance as a control at the clinical dose of 0.1 mmol Gd/kg. Because the contrast-enhanced MRI experiments were noninvasive, the same rats with tumor xenografts were used for testing different agents and doses. All the imaging studies applied the crossover design, with a washout period of at least 3 days. The experiments with MT218 at the dose of 0.04 mmol/kg were performed first, followed by 0.02 mmol/kg MT218 or gadoteridol at 0.1 mmol/kg for the second or third MRI. All animals were euthanized immediately after the last scan.

Magnetic resonance data were exported into digital imaging and communication in medicine files and analyzed using FIJI software. The slice of the tumor was selected based on the contrast levels of the enhanced image. Circular regions of interest (ROIs) of 10 to 20 mm^2 were drawn in the area of the muscle. Another ROI was drawn outlining the tumor. Mean signal intensity in the ROIs was measured in the images. The contrast-to-noise ratio (CNR) in the tumors was calculated using the following equation, $\mathrm{CNR} = \frac{\text{Mean Intensity}_{\text{Tumor}} - \text{Mean Intensity}_{\text{Muscle}}}{\sigma_{\text{noise}}}$, where σ_{noise} is the standard deviation of intensities from an ROI in the lower left corner of the image. The CNR of tumors was calculated before and at 10, 20, and 30 minutes postinjection.

Immunohistochemical Staining

After the last MR image acquisition, the animals were euthanized and tumor tissues were collected for histological and immunohistochemical analyses. Tissue fixation, sectioning, hematoxylin and eosin, and immunohistochemistry staining were performed at the tissue resource core of Case Western Reserve University (Cleveland, OH). Anti-EDB-FN antibody, G4 (Absolute Antibody, Boston, MA), diluted in PBS solution with Tween-20 (PBS-T, 1:100) was applied to the tissue and incubated for 1 hour. Primary antibody detection was performed with Rabbit on Rodent HRP Polymer detection solution for 30 minutes (Biocare Medical, Pacheco, CA). Images were acquired using an Olympus Bx61VS slide scanner (Olympus America, Center Valley, PA) and processed in OlyVIA software.

The Safety Pharmacology

MT218 was evaluated by Eurofins Scientific (San Diego, CA) across a panel of in vitro SAFETYscan E/IC50 assays for potential biological activities in a screen of 78 common biological targets (ADORA2A, ADRA1A, ADRA2A, ADRB1, ADRB2, AVPR1A, CCKAR and CNR1 agonist and antagonist, etc.) over the concentration range of 0.005 to 100 μM following Eurofins' internal standard operating procedures.[33] The assays were performed utilizing the PathHunter enzyme fragment complementation technology, FLIPR-based cellular screening assays, KINOMEscan kinase binding assays, and a variety of enzymatic assays. Positive reference compounds, including NECA and SCH 442416 for ADORA2A calcium flux agonist and antagonist, 61603 hydrobrimide and tamsulosin for ADRA1A calcium flux agonist and antagonist, and UK 14304 and yohimbine for cAMP agonist and antagonist, were assayed in parallel to verify acceptable performance of the assays.

GLP-compliant studies were performed to evaluate the effects of MT218 on the hERG currents, CNS functions in SD rats, and cardiovascular and respiratory system functions in conscious beagle dogs. For the hERG experiment, a Multi Clamp 700B manual patch clamp system (Axon Instruments) was used to induce hERG currents of human embryonic kidney cells HEK293 cell in whole-cell voltage clamp mode. MT218 at 1, 3, 10, 30, and 100 μM or positive control terfenadine at 10 μM was tested. The hERG channel tail currents and the peaks of the tail currents were recorded by Clampex 10.3, and the data were analyzed by Clampfit 10.3.

To evaluate the effects on CNS, 4 groups of (5/sex/group) female and male SD rats received single intravenous (IV) injection of 0, 0.1, 0.3, and 1 mmol/kg. Animals were tested by the functional observational battery assay at 0.25, 0.75, 1.5 and 4 hours after dosing, including home cage observations, hand-held observations, open-field observations, responses to a variety of stimulus, and measurements for grip strength (forelimb) and body temperature. The effects of MT218 injection on cardiovascular and respiratory system functions were explored in conscious beagle dogs following a single IV injection of saline control, MT218 at 0.07, 0.21, and 0.70 mmol/kg in a total of 9 dogs (4 males and 5 females). The dose volume of each animal was 3.5 mL/kg. Electrocardiographic parameters (heart rate, PR interval, QRS duration, QT and QTcF interval, QRS voltage, STe, heart rhythm, and electrocardiogram [ECG] waveform analysis), blood pressure (systolic blood pressure, diastolic blood pressure and mean arterial blood pressure), respiratory frequency, and tidal volume were recorded, analyzed, and evaluated within 1 hour before dosing and at 0.5, 1, 2, 4, and 24 hours after dosing.

Pharmacokinetics

The pharmacokinetics of MT218 was studies in SD rats and beagle dogs after single IV injection of 0.04, 0.1, and 0.2 mmol/kg of MT218 (3 animals/sex). For rats, blood samples were collected from jugular veins at predose and at 2, 5, 10, 15, 30, and 45 minutes and 1, 2, 3, and 4 hours after dosing from group 1 to 3. For dogs, blood samples were collected from fore limb veins at predose and at 5, 10, 15, 30, and 45 minutes and 1, 1.5, 2, 3, 4, and 6 hours after dosing from group 1 to 3. A validated inductively coupled plasma mass spectrometric method (ICP-MS, Agilent 7800) was used for quantitation of Gd concentration in

the plasma. Terbium (Tb) was used as internal standard. Plasma samples (50 μL) and 10 μL IS solution (Tb, 5 μg/mL) were mixed. Then ultrapure water-65% nitric acid-triton X-100 (100:0.1:0.1, v/v/v) was added to dilute samples before analyzed by ICP-MS. Pharmacokinetic parameters, such as half-life $T_{1/2}$, concentration immediately after dosing (C_0), area under the curve (AUC), volume of distribution (V_z), clearance (Cl), mean residence time, and AUC ratio, were calculated by a noncompartment model (noncompartmental analysis) using WinNonlin software (version 8.0).

Biodistribution

For the biodistribution, 30 rats (3/sex/group) received a single IV injection of MT218 at 0.1 mmol/kg. Blood samples and tissues were collected before dosing and 10 and 30 minutes and 2, 6, and 48 hours after dosing. The tissues collected were heart, liver, spleen, lung, kidney, stomach, small intestine, gonads, brain, fat, muscle, submaxillary lymph nodes, prostate (males), skeleton and abdominal skin. Six animals from each group (groups 1–5) were used at each time point. The tissues were homogenized and then digested with nitric acid in Water Bath Constant Temperature Oscillator (Taicang Experimental Equipment Factory & Suzhou Peiying Experimental Equipment Co Ltd). A validated ICP-MS method (Agilent 7800) was used for quantitation of Gd in the rat plasma and tissues. The metabolic parameters were calculated by the noncompartmental analysis using WinNonlin software (version 8.0).

Excretion

The urine, feces, and bile excretion of MT218 was investigated in SD rats after IV injection of 0.1 mmol/kg in a non-GLP study. One group (3/sex) of rats was used for assessing the excretion of the Gd chelate into urine and feces. The feces and urine samples were collected before dosing (D-1) and at 0–4, 4–8, 8–24, 24–48 (D1–D3), 48–72 (D3–D4), 72–96 (D4–D5), 96–120 (D5–D6) and 120–144 (D6–D7) hours after dosing. The second group was used for assessing bile excretion using conscious biliary cannulation. The bile was collected 30 minutes predose and 0–1, 1–2, 2–4, 4–6, 4–6, and 6–8 hours after dosing. Gd content in the samples was determined by ICP-MS (Agilent 7800).[34]

Toxicity

Single and repeated toxicity was performed under GLP conditions in SD rats and beagle dogs. Rats were 6 to 7 weeks old and weighed 200 to 246 g for males and 175 to 224 g for females on day -1 (Beijing Vital River Laboratory Animal Technology Co, Ltd). Male dogs were 6 to 7 months old and weighed 7.34 to 10.58 kg. Female dogs were 6 to 7 months old and weighed 6.50 to 9.87 kg on day −1 (Marshall Biotechnology [Gu'an] Co, Ltd). The toxicity, toxicokinetic profile, and potential target organs' toxicity and tissue distributions of MT218 were investigated after a single IV injection at a dose of 1.39 mmol/kg or daily IV injection for 2 weeks at doses of 0.15, 0.46, and 1.39 mmol/kg/d in rats; and at a single dose of 0.70 mmol/kg or daily injection at 0.07, 0.21, and 0.70 mmol/kg/d for 2 weeks in dogs according to the study design listed in Table 1. Saline injection was used as a placebo control. The animals were observed during and after the injections for potential side effects. The reversibility of any potential toxicity was monitored during an additional 2-week recovery period. Parameters evaluated in the study included dose formulation analysis, mortality and moribundity, clinical observations, body weights, food consumption, body temperature, ophthalmoscopic examinations, hematology, coagulation, clinical chemistry, urinalysis, plasma drug concentration, and toxicokinetic analysis. At the end of the recovery period, the animals were euthanized, and tissues and organs were collected and weighed and then subjected to macroscopic and microscopic histological examinations for any sign of toxic side effects. Rat tissues of the bone (femur), skin (abdomen), liver, brain, muscle (quadriceps femoris), lung, heart, kidney, spleen, large intestine (colon), and small intestine (jejunum) were collected at scheduled necropsy on day 29 for groups 1 to 4 and day 15 for single-dose group 5 to test the Gd remaining in the tissues using a well-established ICP-MS method. The no observed adverse effect level (NOAEL) was determined as the highest dose at which there are no biologically significant increases in the frequency or severity of adverse effect between the test and control groups.

TABLE 1. Design and Group Assignment of Rat and Dog Toxicity Studies

Group	Control/ MT218	Dose Level, mmol/kg/d	Number of Animals/Sex	Notes
Rat toxicity				
1	Control	0	5 + 10 + 5*	Repeated dose
2	MT218	0.15	10 + 5†	
3	MT218	0.46	10 + 5†	
4	MT218	1.39	10 + 5†	
5	MT218	1.39	5 + 5‡	Single dose
6	Control	0	4 + 2§	Toxicokinetics
7	MT218	0.15	8 + 2§	
8	MT218	0.46	8 + 2§	
9	MT218	1.39	8 + 2§	
Dog toxicity				
I	Control	0	3 + 3 + 2‖	Repeated dose
II	MT218	0.07	3 + 2¶	
III	MT218	0.21	3 + 2¶	
IV	MT218	0.70	3 + 2¶	
V	MT218	0.70	3 + 2#	Single dose

*The first 5 animals per sex were designated for the necropsy on day 3, the middle 10 animals per sex were designated for the necropsy after 2 weeks of dosing, and the last 5 animals per sex were designated for necropsy after the 2 week recovery period following the last dosing.

†The first 10 animals per sex per group in groups 2–4 were designated for the necropsy after 2 weeks of dosing. The last 5 animals per sex per group were designated for necropsy after the 2-week recovery period after the last dosing.

‡The first 5 animals per sex were designated for the necropsy on day 3 and the last 5 animals per sex per group were designated for necropsy on day 15.

§The last 2 animals per sex per group were included as TK replacement animals and received dosing. They were euthanized after the last blood sample collection.

‖The first 3 animals per sex were designated for the necropsy on day 3, the next 3 animals per sex were designated for the necropsy after 2 weeks of dosing on day 15, and the last 2 animals per sex were designated for necropsy after the 2-week recovery period after the last dosing on day 29.

¶The first 3 animals per sex per group were designated for necropsy after 2 weeks of dosing. The rest 2 animals per sex per group were designated for necropsy after the 2-week recovery period after the last dosing.

#The first 3 animals per sex were designated for the necropsy on day 3 and the remaining 2 animals per sex per group were designated for necropsy on day 15.

Genotoxicity and Other Toxicity Studies

Genotoxicity of MT218 was evaluated using a *S. typhimurium* mutagenicity test, a chromosomal aberration test in CHL fibroblasts, and in vivo, a micronucleus assay in Institute of Cancer Research (ICR) mice. The mutagenicity of MT218 injection was evaluated in TA97a, TA98, TA100, TA102, and TA1535 at the dose level of 15, 50, 150, 500, 1500, and 5000 μg/plate. The vehicle control (sodium chloride injection); positive controls of direct mutagens 9-aminoacridine (50 μg/plate), 2-nitrofluorene (10 μg/plate), sodium azide (6 μg/plate), and 4-nitroquinoline *N*-oxide (1 μg/plate); and indirect mutagens 2-aminoanthracene (3 μg/plate) and benzopyrene (5 μg/plate) were also included in the test. The potential genotoxicity of MT218 injection to induce chromosomal aberration in CHL fibroblast with or without rat liver S9 metabolic activation was evaluated at 2000, 1000, and 500 μg/mL for 4 or 27 hours. The vehicle control

(sodium chloride injection) and positive controls of direct clastogen mitomycin C at 0.1 μg/mL and indirect clastogen cyclophosphamide monohydrate at 10 μg/mL were also included in the test. One hundred or 300 well-spread metaphase cells per treatment were evaluated, and chromosomal aberration ratio for each treatment was calculated.[35] The micronucleus assays in ICR mice were tested in a total of 32 male ICR mice (Vital River Laboratories Co, Beijing, China), with 8 mice per group in the 2000 mg/kg/d group and 6 mice per group in the vehicle control and 500 and 1000 mg/kg/d test groups. Cyclophosphamide monohydrate was used as positive control. The animals of all groups were dosed once daily for 2 days, and bone marrow was collected analyzed at about 22.5 hours after the final dose from all animals.[35]

Other GLP-compliant toxicology studies included an in vitro hemolysis test for MT218 using rabbit red blood cells (RBCs) and assessment of the potential for active systemic anaphylaxis of MT218 using guinea pigs. For the in vitro hemolysis test, 0.1, 0.2, 0.3, 0.4, and 0.5 mL of MT218 at 0.2 mol/L was incubated with 2.5 mL of 2% rabbit RBC suspension at 37°C ± 0.5°C, with saline and sterile water as negative and positive control. Hemolysis and aggregation were recorded at 15, 30, and 45 minutes and 1, 2, and 3 hours after incubation. For the potential active systemic anaphylaxis, a total of 36 male guinea pigs were randomly assigned to 4 groups (9 animals/group): saline group, human albumin group (40 mg/kg for sensitization, and 80 mg/kg for challenge), and 2 MT218 dose groups (0.200 and 0.695 mmol/kg for sensitization and doubled concentrations for challenge.) Animals were sensitized by intraperitoneal injection on days 1, 3, and 5. Fourteen days after last sensitization injection (day 19), the first 3 animals of each group received foot IV injection challenge. The rest animals of each group were challenged 21 days after last sensitization injection (day 26). Animals were observed twice daily (AM and PM) during the study period for signs of mortality, mental state, behavior, morbidity, respiration, secretion, feces, and capability of water and food intake. Body weights were recorded before, during, and at the end of the study.

RESULTS

Relaxivity and Binding Affinity of MT218

The r_1 and r_2 relaxivities of MT218 are listed in comparison with r_1 relaxivity of gadoteridol in Table 2. The r_1 relaxivity of MT218 was nearly 2-fold of that of gadoteridol, but the r_1/r_2 ratio is similar to gadoteridol. The relaxivities did not change substantially when the magnetic field strength increased from 1.4 to 3.0 T. The results were the same as for the previously reported relaxivities.[26] The r_1 relaxivity of MT218 was also significantly higher than that of the prototype agent ZD2-Gd(HP-DO3A) (4.12 mM^{-1} s^{-1} at 1.4 T) that used a $(CH_2CH_2O)_2$ spacer. The increased relaxivity might be attributed to the more rigid spacer, a 5-membered triazole ring, between the peptide and Gd(HP-DO3A), which probably deceases the rotational rate of the chelate.[38,39] The binding affinity constant (K_d) of MT218 to the EDB fragment was measured in the range from 0.76 to 6.88 μM, with the average binding affinity of 3.45 μM (n = 4). The moderate binding affinity enables a rapid binding of the agent to the ECM oncoprotein at the clinically expected GBCA and EDB-FN concentrations and would allow reversible binding of the agent to facilitate rapid clearance from the body after imaging.

TABLE 2. Relaxivities of MT218

Contrast Agent	Magnetic Field	r_1 Relaxivity, mM^{-1} s^{-1}	r_2 Relaxivity, mM^{-1} s^{-1}
Gadoteridol	1.4 T[36]	3.2 (H_2O)	
	1.5 T[37]	2.9 (H_2O)	3.2 (H_2O)
		4.1 (plasma)	5.0 (plasma)
	3.0 T[37]	2.8 (H_2O)	3.4 (H_2O)
		3.7 (plasma)	5.7 (plasma)
MT218	1.4 T	5.34 (H_2O)	7.40 (H_2O)
		6.58 (PBS)	8.87 (PBS)
		6.54 (HSA)	8.70 (HSA)
	3.0 T	6.25 (H_2O)	7.90 (H_2O)
		6.16 (PBS)	7.91 (PBS)

PBS indicates phosphate-buffered saline; HSA, human serum albumin.

Chelation Stability

The Gd(III) chelation stability of MT218 was determined by challenging the chelate with different chelating ligands and Zn^{2+} ions.[40] MT218 is highly stable, at least kinetically, at neutral pH 7.4 and no transmetallation or dissociation of MT218 was observed in the presence of DOTA, DTPA, HP-DO3A, EDTA, and Zn(II) at pH 7.4 and the temperature of 25°C and 37.5°C for 1 month (Fig. 2A). At pH 5 and 25°C, MT218 also showed chelation stability for at least 30 days. MT218 was stable at pH 5 and 37.5°C in acetate buffer (Fig. 2B). Loss of MT218 was observed at pH 5 and 37.5°C in the presence of the free chelating ligands, DOTA, DTPA, HP-DO3A, and EDTA, probably because of competitive acid-assisted dissociation of the Gd(III) from MT218 (Fig. 2C). Nevertheless, the presence of Zn(II) ions did not cause dissociation of MT218 at pH 5 and 37.5°C for at least 30 days (Fig. 2D).

Plasma Protein Binding and Stability

After a short incubation (3 minutes) of MT218 with rat, dog, and human plasma, the binding ratios of the agent to plasma proteins was determined by the concentration of the bound MT218 to the total concentration in the solutions. The binding ratios were 28.44%, 27.12%, and 25.68% in rat plasma, 29.10%, 26.91%, and 48.44% in dog plasma, and 47.31%, 45.15%, and 40.50% in human plasma at concentrations of 50, 80, and 110 μM, respectively (n = 4). To test the stability of the peptide in MT218, the agent was incubated in PBS and rat, dog, and human plasma at 37°C for up to 48 hours. After incubating MT218 for 1, 3, 6, 28, and 48 hours, the average remaining percentage of intact MT218 was 74.87%, 20.54%, 4.61%, 0%, and 0% in rat plasma; 89.19%, 71.45%, 47.81%, 11.23%, and 5.38% in dog plasma; and 83.47%, 48.79%, 12.87%, 5.21%, and 3.97% in human plasma, respectively (Fig. 3) (n = 2). The enzymatic degradation half-life ($t_{1/2}$) of MT218 was 1.63, 5.85, and 2.63 hours in rat, dog, and human plasma, respectively. The results indicate that the ZD2 peptide in MT218 undergoes enzymatic cleavage by peptidases in plasma. The peptide degraded more rapidly in rat plasma than dog and human plasma.

In Vitro Metabolism

A metabolic stability study was conducted to examine whether MT218 remained stable during incubation with hepatocytes. After 2 hours of incubation with the hepatocytes from human, CD1 mouse, SD rat, beagle dog, or cynomolgus monkey, the remaining MT218 was 61.1%, 50.6%, 67.5%, 41.0%, 82.9%, respectively, indicating that MT218 was partially metabolized in hepatocytes from these species. The remaining MT218 in negative control was 100% after 2 hours of incubation. The remaining testosterone and 7-hydroxycoumarin in the positive control were 9.29% and 18.8%, respectively.

Two metabolites were identified after incubation with the above hepatocytes, both resulting from the hydrolysis of the peptide moiety. A metabolic pathway study was then carried out to assess whether CYP450 enzymes were involved in the metabolism of MT218 using human liver microsomes. In the systematic control, the remaining testosterone was 11.4% after incubating with the human liver microsomes for 120 minutes. The MT218 remaining was 105%, 117%, 101%, 98.8%, 105%, 109%, and 99.1% after incubating 1 μM MT218 with human liver microsomes for 2 hours for the CYP1A2, CYP2B6,

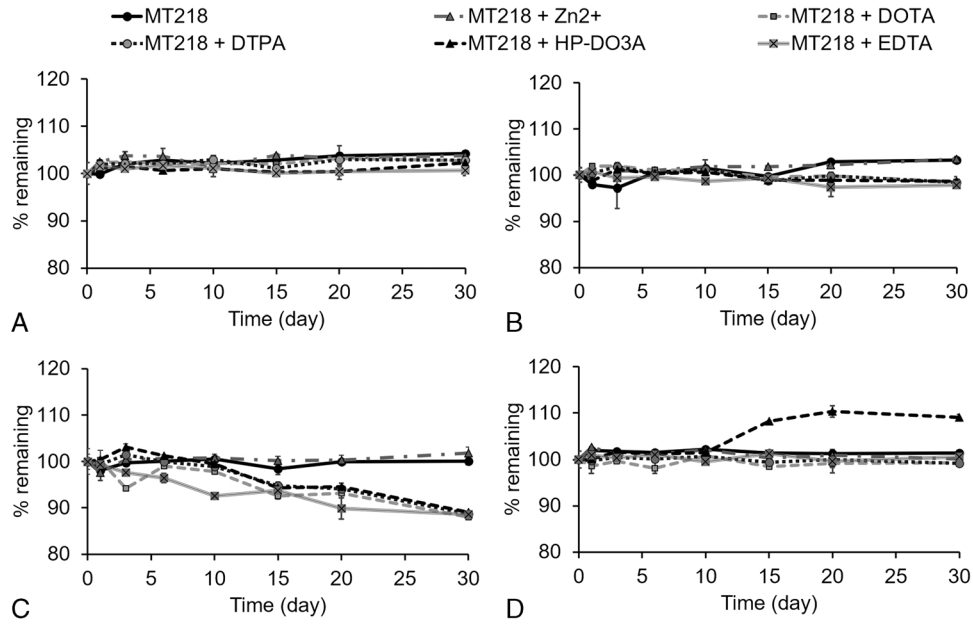

FIGURE 2. Percentage of MT218 remaining in the mixture solution under the challenge of $ZnCl_2$, DOTA, DTPA, HP-DO3A, and EDTA at pH 5 or 7.4 and a temperature of 25°C or 37.5°C, respectively. A, pH 5, 25°C, (B) pH 7.4, 25°C, (C) pH 5, 37.5°C, (D) pH 7, 37.5°C. The final concentration of MT218, DOTA, DTPA, HP-DO3A, and EDTA in the mixture solution was 0.25 mM. The final concentration of $ZnCl_2$ in the mixture solution was 0.50 mM.

CYP2C8, CYP2C9, CYP2C19, CYP2D6, and CYP3A4 groups, respectively, suggesting that the CYP450 enzymes were not involved in the metabolism of MT218.

MT218's potential inhibition effect on CYP450 enzymes was tested at the concentrations of 0.01, 0.1, 1, 10, and 100 μM. In the positive control, the enzyme activities of CYP1A2, 2B6, 2C8, 2C9, 2C19, 2D6, and 3A4 were decreased to 25.2%, 10.8%, 20.0%, 12.6%, 15.1%, 8.85%, and 8.30% when incubated with the selective inhibitors of CYP450, which were α-naphthoflavone (for CYP1A2), thiotepa (for CYP2B6), montelukast (for CYP2C8), sulfaphenazole (for CYP2C9), ticlopidine (for CYP2C19), quinidine (for CYP2D6), and ketoconazole (for CYP3A4), respectively. After incubation with liver microsomes, the corresponding enzyme activities were decreased by 74.8%, 89.2%, 80.0%, 87.4%, 84.9%, 91.2%, and 91.7%, respectively, indicating that the test systems were qualified for this study. MT218 did not inhibit the activities of CYP1A2, CYP2B6, CYP2C9, CYP2C19, CYP2D6, or CYP3A4 from human liver microsomes. MT218 showed inhibition potential to CYP2C8, and the relative activities decreased to 52.5% of the negative controls at the highest test concentration, which suggested that the IC50 value was greater than 100 μM.

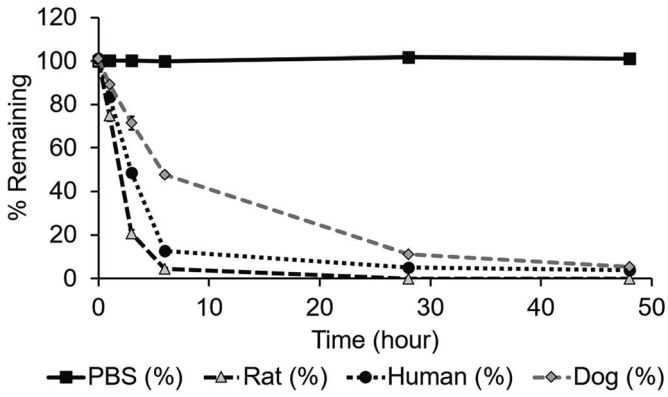

FIGURE 3. Percentage remaining of MT218 in the PBS, rat plasma, human plasma, and dog plasma after incubating at 37°C for 48 hours.

MT218's inhibition of the human ATP-binding cassette (ABC) transporters and solute carrier (SLC) transporters was explored at the concentrations of 1, 5, 10, 50, and 100 μM. MT218 displayed no inhibition potential on the transporter activities of MDR1, BCRP, OATP1B1, OATP1B3, OAT1, OAT3, OCT2, MATE1, and MATE2K. The positive controls inhibited 97.4% and 98.9% of MDR1 and BCRP transporter activities, respectively. The negative controls showed that the substrate uptake ratios by OATP1B1, OATP1B3, OAT1, OAT3, OCT2, MATE1, and MATE2K were between 78.5% and 126%, whereas substrate uptake ratios for MT218 were between 79.0% and 100%, and the uptake ratios for positive controls were between 0% and 16.3%.

In the study investigating the induction potential of MT218 on the enzyme activity and mRNA expression of CYP1A2, CYP2B6, and CYP3A4 using human primary hepatocytes, MT218 exhibited no induction on enzyme activity of CYP1A2, CYP2B6, and CYP3A4 at concentrations of 1, 10, and 100 μM. In the positive controls, omeprazole, phenobarbital, and rifampicin inducted about 40-, 12-, and 15-fold increase of enzyme activity in comparison with vehicle control. MT218 did not induce the mRNA expression of CYP2B6 and CYP3A4 at concentrations of 1, 10, and 100 μM. Omeprazole, phenobarbital, and rifampicin inducted about 62-, 14-, and 60-fold increase of mRNA expression in comparison with vehicle control. However, MT218 might have potential induction on the mRNA expression of CYP1A2 at the high concentration of 100 μM. The mRNA expression levels of CYP1A2 in the incubation system of human hepatocytes with MT218 was more than 2-fold (2.10-fold) of the vehicle controls at the test concentration of 100 μM from 1 of the 3 lots of cells.

Dosing Effect of MT218 for MRMI of Prostate Cancer in Rat Models

The dosing effect of MT218 was assessed in the rats bearing aggressive PC3 human prostate cancer xenografts with high EDB-FN expression and slow-growing LNCaP human prostate tumors with low EDB-FN expression. Figure 4 shows the T_1-weighted 2D spin-echo MR images and CNR of the tumors before and at different time points

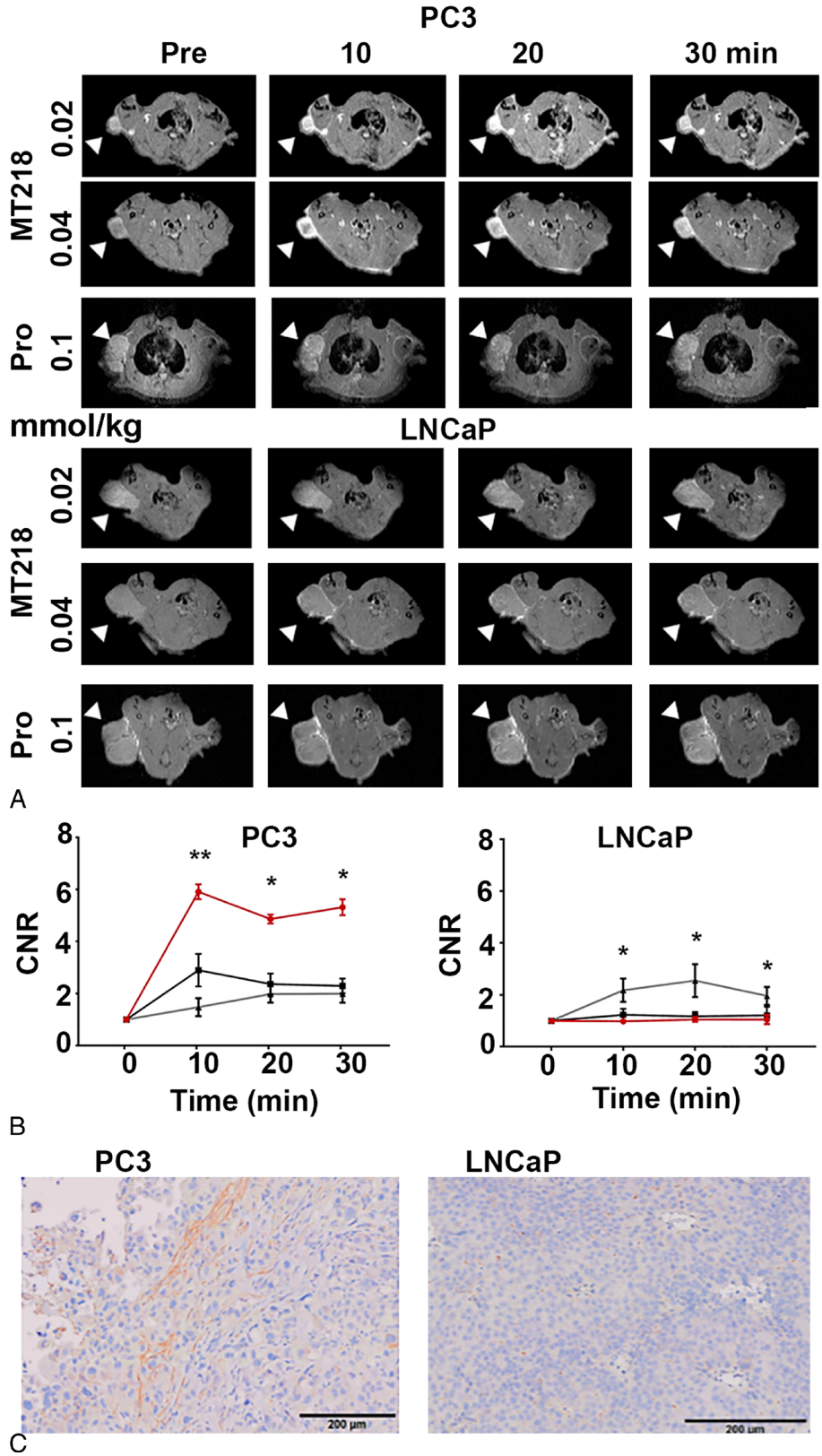

FIGURE 4. Representative T_1-weighted spin-echo axial MR images (A) and average CNR (B) of PC3 (n = 6) and LNCaP (n = 3) prostate tumor xenografts in rats before and at 10, 20, and 30 minutes postinjection of MT218 at 0.02 mmol/kg (black, ■) and 0.04 mmol/kg (red, ●) and gadoteridol (Pro) at 0. 1 mmol/kg (gray, ▲) and immunohistochemical staining of EDB-FN (C) in the tumors (bar, 200 µm). The imaging experiment was initiated at 5 and 6 weeks after implantation of PC3 and LNCaP cells, respectively. *$P < 0.05$, **$P < 0.01$.

after IV injection of MT218 at 0.04 or 0.02 mmol/kg and gadoteridol at 0.1 mmol/kg. MT218 produced strong signal enhancement in the PC3 tumors (CNR, 5.94 ± 1.68) at 10 minutes postinjection of 0.04 mmol Gd/kg. The strong tumor enhancement persisted for at least 30 minutes (CNR, 4.92 ± 0.79) even though MT218 had a short elimination half-life in rat plasma owing to fast degradation (Fig. 3). Substantial contrast enhancement was still observed in PC3 tumors with MT218 at 0.02 mmol Gd/kg at 10 minutes (CNR, 2.67 ± 1.05) and 30 minutes (1.97 ± 0.67) postinjection, respectively. Significantly more signal enhancement was also observed for MT218 at 0.02 mmol/kg than gadoteridol at 0.1 mmol/kg in PC3 at 10 minutes. The CNR with gadoteridol was 1.32 ± 0.58 at 10 minutes and 1.714 ± 0.69 at 30 minutes postinjection, respectively. MT218 at both doses resulted in little enhancement in LNCaP tumors of low EDB-FN expression, with a CNR of 1.13 ± 0.38 at the dose of 0.04 mmol/kg and 0.88 ± 0.06 at 0.02 mmol/kg. Interestingly, gadoteridol produced higher signal enhancement than MT218 in LNCaP tumors, with CNR of 1.79 ± 0.74, owing to its higher dose. The expression of EDB-FN in the tumors was determined by immunohistochemical staining. EDB-FN was significantly upregulated in the aggressive PC3 prostate tumors. In contrast, the slow-growing LNCaP

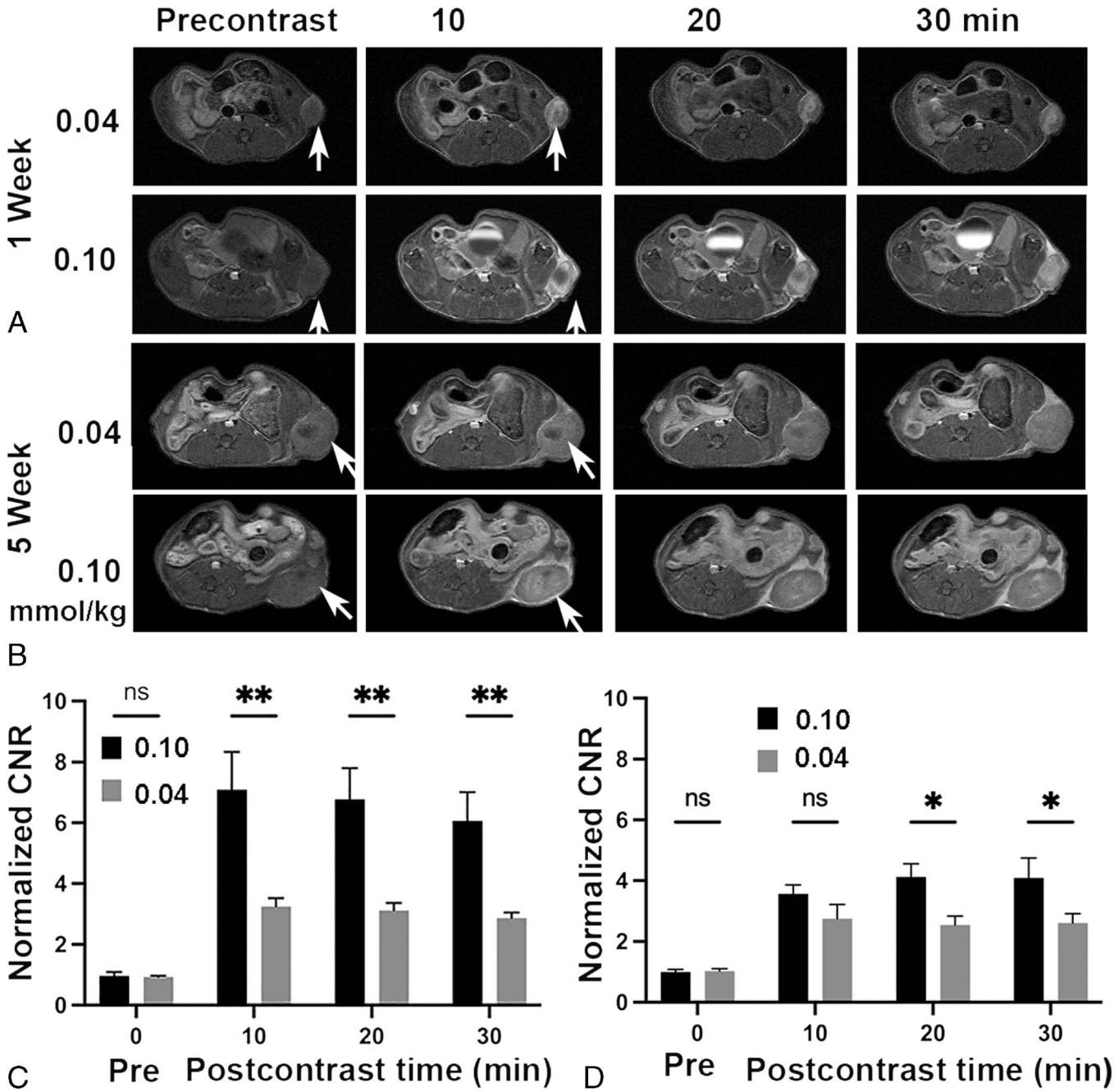

FIGURE 5. Representative T_1-weighted spin-echo axial MR images (A, B) and average CNR (C, D) of murine KPC pancreatic cancer allografts in C57BL/J6 immunocompetent mice at approximately a week (A, C) and 5 weeks (B, D) after tumor initiation and before and at 10, 20, and 30 minutes postinjection of MT218 at 0.04 or 0.1 mmol/kg (n = 5). *$P < 0.05$; **$P < 0.01$.

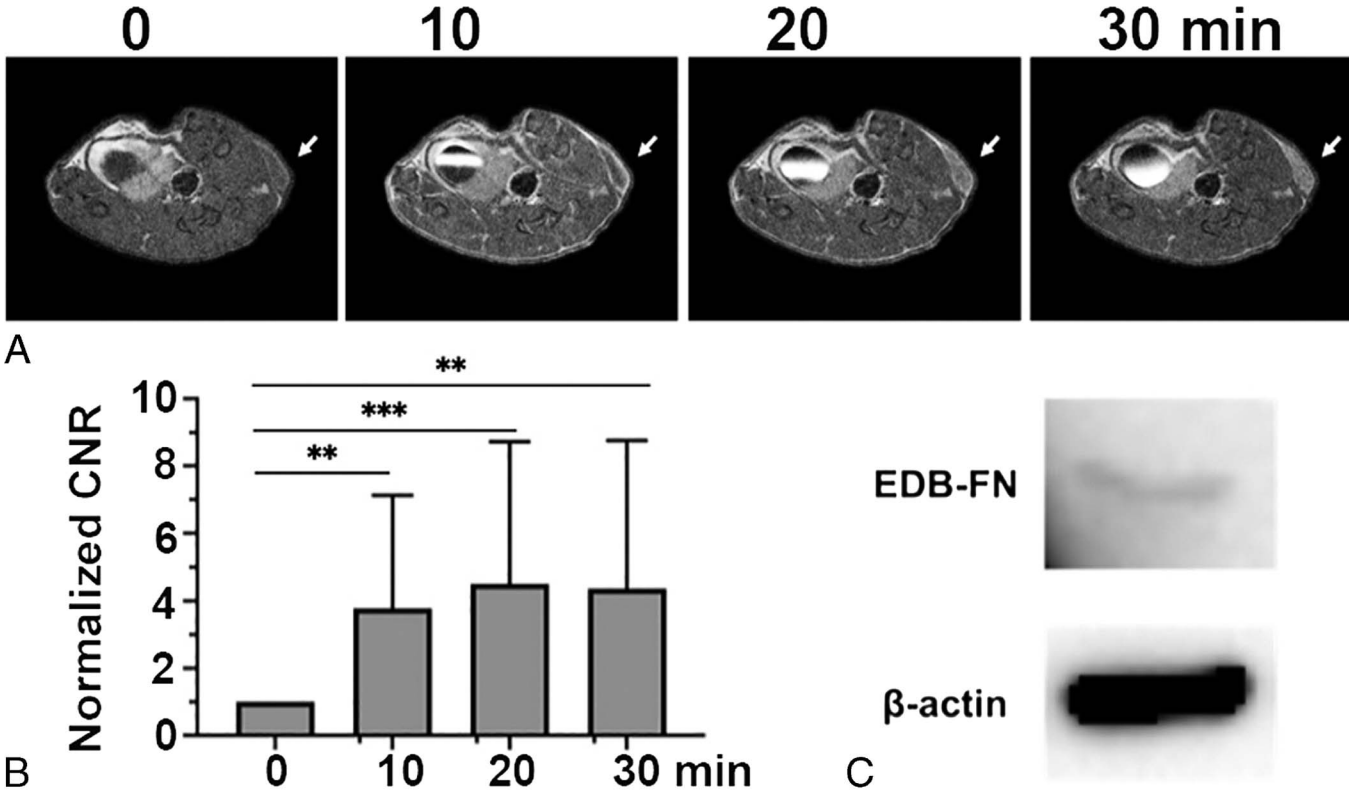

FIGURE 6. Representative T_1-weighted spin-echo axial MR images (A) and average CNR (B) of H1299 lung tumor xenografts in nude mice before and at 10, 20, and 30 minutes postinjection of MT218 0.04 mmol/kg and western blots (C) of EDB-FN in the cultured H1299 cells (n = 6). $^{**}P < 0.01$; $^{***}P < 0.001$.

tumors exhibited little expression of EDB-FN (Fig. 4C). The results showed that MT218 produced robust tumor enhancement in the aggressive prostate tumors with high EDB-FN expression at substantially reduced doses and has a potential to differentiate invasive from noninvasive prostate tumors.

Dosing Effect of MT218 for MRI Murine Pancreatic Cancer in Mice

Pancreatic cancer generally has dense tumor stroma that is difficult to overcome to deliver molecular imaging agents for diagnostic imaging. In recent studies, it has been shown that MT218 is effective in producing robust contrast enhancement in both orthotopic and metastatic pancreatic cancer in mouse models at a dose of 0.1 mmol/kg.[30,41] Here, we assessed the dosing effect of MT218 for MRMI of pancreatic cancer in immune competent mice bearing subcutaneous KPC murine tumors of different sizes or stages. Once primary tumors reached about 100 mm^3 (~1 week), MRMI was performed before and after IV injection of MT218 at a dose of 0.1 or 0.04 mmol/kg. In both cases, the strongest tumor contrast enhancement was seen at 10 minutes postinjection. MT218 produced about 7-fold CNR increase over the precontrast CNR at 0.1 mmol/kg and a 3.3-fold increase at 0.04 mmol/kg (Fig. 5A, C). Strong tumor enhancement persisted for at least 30 minutes for both doses. At week 5, when tumors were larger and denser, MT218 still produced substantial enhancement across the tumor tissues at both doses when compared with precontrast tumor images. There was no significant difference in CNR enhancement between 2 doses at 10 mins (3.6-fold vs 2.8-fold). About a 4-fold CNR increase was observed in the tumors at 20 and 30 minutes postcontrast at 0.1 mmol/kg, significantly higher than the CNR increase at 0.04 mmol/g (ca. 2.6) (Fig. 5B, D). The results demonstrate that MT218 is able to produce robust tumor enhancement in pancreatic cancer with significant

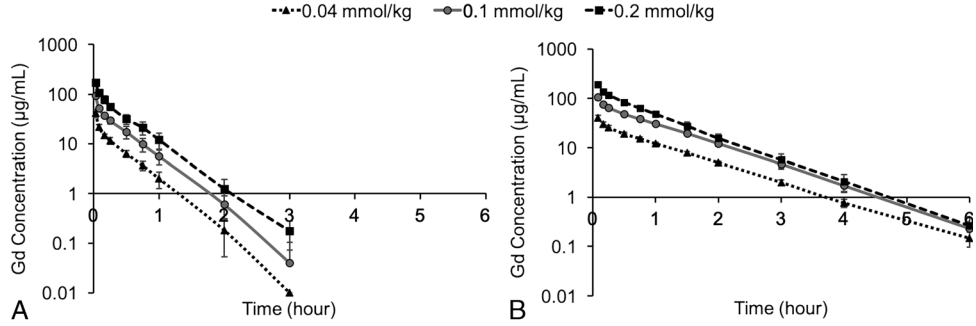

FIGURE 7. Logarithmic plasma concentration-time curves of MT218 in rats (A) and beagle dogs (B).

TABLE 3. Pharmacokinetic Parameters of MT218 Based on Gd(III) Measurement in SD Rats and Beagle Dogs

	Dose, mmol/kg	Sex	$T_{1/2}$, h	C_0, μg/mL	AUC h×μg/mL	AUC_{INF}, h×μg/mL	V_z, mL/kg	Cl, mL/h/kg	MRT, h	AUC Ratio
Rat	0.04	♂	0.30	49.09	11.08	11.18	243.09	578.42	0.37	1
		♀	0.28	75.09	10.94	11.13	224.22	568.10	0.29	1
		P	0.57	0.02*	0.93	0.97	0.29	0.89	0.13	
	0.1	♂	0.31	115.85	28.86	29.01	240.18	550.32	0.40	2.61
		♀	0.32	158.07	27.84	28.02	273.35	575.39	0.34	2.55
		P	0.65	0.01*	0.81	0.81	0.60	0.78	0.28	
	0.2	♂	0.30	248.60	53.17	53.23	255.24	591.30	0.37	4.80
		♀	0.32	209.22	58.60	58.71	256.40	552.59	0.43	5.36
		P	0.22	0.33	0.51	0.51	0.97	0.60	0.28	
Dog	0.04	♂	0.76	50.97	34.80	34.94	197.08	180.20	1.01	1
		♀	0.74	59.33	38.16	38.47	175.99	164.04	0.97	1
		P	0.80	0.32	0.10	0.10	0.30	0.10	0.58	
	0.1	♂	0.70	149.33	89.52	89.78	177.73	175.72	0.95	2.57
		♀	0.67	146.59	93.96	94.17	161.08	167.64	0.96	2.46
		P	0.33	0.93	0.46	0.47	0.10	0.47	0.85	
	0.2	♂	0.69	286.90	156.54	156.90	201.64	202.02	0.88	4.50
		♀	0.63	268.10	138.99	139.15	205.93	226.54	0.79	3.64
		P	0.048*	0.64	0.18	0.18	0.76	0.18	0.20	

AUC ratio = $AUC_{(middle, high dose)}$ / $AUC_{(low dose)}$ For rats, the AUC is 0-4h, for dogs, the AUC is 0-6h. *P* value: independent *t* test, female vs male. n = 3 animals per dose per sex. Cl is clearance, whereas V_z is volume of distribution.

SD indicates Sprague-Dawley; AUC, area under curve; MRT, mean residence time.

* $P < 0.05$: statistical difference between male and female animals.

CNR increase at the reduced dose (0.04 mmol/kg) for potentially detecting pancreatic cancer.

MRMI of Lung Cancer With MT218 at a Reduced Dose

The efficacy of MT218 for MRMI of lung cancer was assessed in nude mice bearing H1299 human non–small cell lung cancer xenografts at 0.04 mmol Gd/kg. Strong enhancement was seen in the periphery of the tumors at 10 minutes postinjection and substantial signal enhancement was then observed in the inner tumor tissue at 20 and 30 minutes, indicating gradual diffusion of MT218 into the inner tumor tissues (Fig. 6A). An average of 3- to 4-fold CNR increase was measured in the tumor tissues from 10 to 30 minutes postinjection (Fig. 6B). The

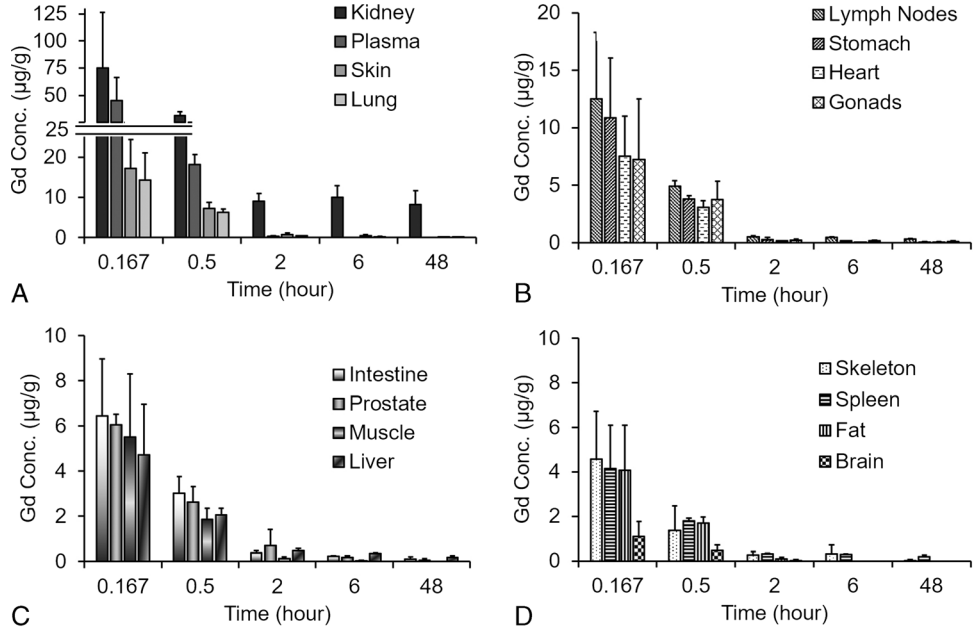

FIGURE 8. Concentration of Gd in rat plasma and major tissues over the period of 48 hours after injection of 0.1 mmol/kg MT218. Kidney, plasma, skin and lung (A); lymph nodes, stomach, heart and gonads (B); intestine, prostate, muscle, and liver (C); skeleton, spleen, fat and brain (D). The Gd concentration in the tissues was determined by ICP-MS.

TABLE 4. Summary of AUC and C_{max} Parameters of MT218 Based on Gd Measurement in Rat Plasma and Major Tissues

Tissue	C_{max}, μg/mL or μg/g	$AUC_{(0–48h)}$, h×μg/g or h×μg/mL	AUC_{INF}, h×μg/g or h×μg/mL
Kidney	74.89	481.54	2936.07
Plasma	44.96	34.06	34.18
Skin	17.21	28.54	30.96
Lymph nodes	12.53	27.63	51.39
Lung	14.28	17.81	19.50
Liver	4.73	17.22	27.86
Spleen	4.14	15.18	35.21
Small intestine	6.44	13.99	19.76
Stomach	10.87	12.99	15.13
Prostate	6.05	12.05	13.12
Skeleton	4.58	11.83	12.16
Gonads	7.22	11.78	17.48
Heart	7.54	7.15	7.56
Muscle	5.51	4.27	4.29
Fat	4.07	3.18	3.23
Brain	1.10	0.86	0.87

AUC indicates area under curve.

expression of EDB-FN protein was shown in H1299 cells by Western blotting (Fig. 6C). The results suggest that MT218 has a potential for MRMI of lung cancer.

Safety Pharmacology

In comparison with positive control, MT218 did not exhibit any notable target-specific secondary pharmacologic activity in an in vitro assay with a 78-target panel in the concentration range of 0.005 to 100 μM. MT218 showed some inhibition activity on targets of HRH1, CNR2, OPRD1, CAV1.2, GABAA, and MAOA, with inhibition rates of 17.77%, 12.4%, 11.08%, 15.58%, 24.25%, and 10.21%, respectively. The inhibition rate of all other 72 targets ranged from 0% to 8.2% with majority of zero inhibition.

At 30.69 and 103.54 μM, MT218 inhibited the hERG currents with an average inhibition of 36.87% ± 6.93% and 52.19% ± 0.82%, respectively, whereas the positive control terfenadine at 10 μM exhibited 98.40% ± 0.31% inhibition of the hERG currents. No abnormal ECG waveform or rhythm was observed during electrocardiographic analysis after MT218 dosing in beagle dogs. There was no MT218-related effect for parameters of ECG (PR interval, QRS duration, QT interval, QTcF interval, QRS voltage, STe, heart rhythm, and ECG waveform), blood pressure (systolic blood pressure, diastolic blood pressure, and mean arterial blood pressure), or respiratory function (respiratory frequency and tidal volume) following administration of 0.07, 0.21, or 0.70 mmol/kg MT218. No MT218-related effect on parameters of CNS function was found after a single IV injection with MT218 at doses of 0.1, 0.3, and 1.0 mmol/kg in SD rats.

Pharmacokinetics

Figure 7 shows the logarithmic plasma concentration-time curves after IV administration of MT218 at 0.04, 0.1, and 0.2 mmol/kg in rats and dogs. Pharmacokinetic parameters in rats and dogs are listed in Table 3. MT218 was cleared from circulation with the mean plasma elimination half-life ($t_{1/2}$) of 0.31 and 0.69 hours in rats and dogs at 0.1 mmol/kg, respectively. The elimination half-lives of MT218 were similar to those of gadoteridol, approximately 0.39 and 0.78 hours in rats and dogs, respectively.[42] The dose increase did not affect the elimination half-life, clearance rate (Cl) and volume of distribution (V_z) in both species. In both rats and dogs, the area under curve (AUC) showed a dose-dependent linear increase. There was no significant difference in $t_{1/2}$ between sexes in rats and low- and medium-dose dog groups, whereas a significant difference was found between male and female dogs at 0.2 mmol/kg ($P < 0.05$).

Biodistribution

The Gd concentration in 15 major tissues and plasma up to 48 hours after IV injection of 0.1 mmol/kg MT218 in SD rats is shown in Figure 8. Relatively high Gd concentration was found in the kidneys possibly because of the fact that the agent was mainly excreted via renal filtration. Low levels of Gd were detected near the lower limit of quantitation (LLOQ; 0.1 μg/g) of ICP-MS in most organs at 48 hours, indicating MT218 cleared fast from other tissues and organs. The AUC and C_{max} parameters are shown in Table 4. Gd was mainly distributed in the kidneys, followed by the plasma, submaxillary lymph nodes, small intestine, skin, lung, liver, gonads, spleen, and bone, with relatively low exposure in the stomach, prostate, body fat, heart, muscle, and brain. In the brain, the Gd concentration was the lowest among all organs and tissues and reached LLOQ at 2 hours and became undetectable at 6 hours post-injection.

Excretion

The percentage excretion of injected MT218 (% inj. Gd) in rat urine, feces, and bile at 6 days after a single IV injection of 0.1 mmol/kg MT218 is shown in Figure 9A. The contrast agent was mainly excreted via kidneys into urine, whereas a small amount was excreted by feces and bile. In urine, Gd excretion reached the maximum during the 8- to 24-hour period (Fig. 9B). The total excretion of injected Gd in bile, feces, and urine was 100.01% ± 10.85% of the injected dose within 6 days. There was no significant sex difference between the total excreted urine Gd ($P > 0.05$).

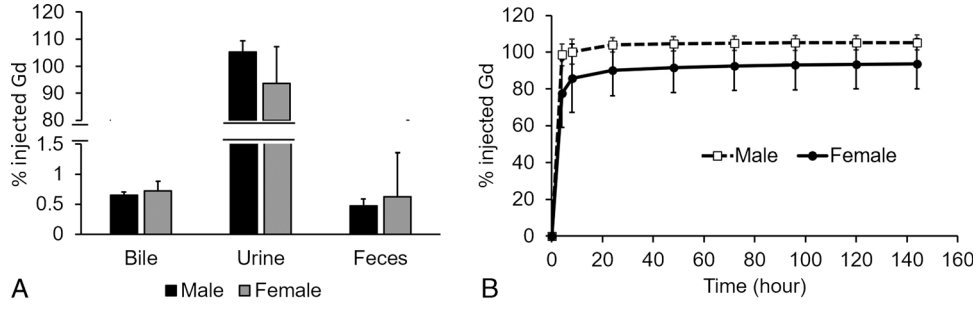

FIGURE 9. Excretion of MT218 in rat urine, feces, and bile 6 days after IV injection of 0.1 mmol/kg (A). MT218 excretion in urine within 6 days after IV injection of 0.1 mmol/kg (B). The Gd concentration in the tissues was determined by ICP-MS.

Single- and Repeated-Dose Toxicology

No mortality or moribundity was noted in the rats and dogs in any dose group during the dosing observations. No MT218-related changes were observed in clinical observations, including body weight, food consumption, body temperature, ophthalmoscopy, hematology, coagulation, clinical chemistry, and urinalysis at any dose level in rats and dogs. Sporadic symptoms of emesis, retching, and salivation were noted in the single- and repeated-medium and high-dose dog groups during the dosing period. The symptoms disappeared after dosing completion. Pathological investigation at the end of the experiments revealed that no MT218-related macroscopic and microscopic abnormality was noted in the rats that received a single dose (1.39 mmol/kg). In the rats that received repeated high doses (1.39 mmol/kg/d), vacuolation of tubular epithelial cells (proximal and distal tubules) with some degenerative changes was observed at the terminal euthanization (day 15). This histological change was still present at the end of recovery period (day 29). No such abnormality was observed in the rats in the low and medium repeated-dosing groups. In dogs, a mild bilateral tubule degeneration of proximal and distal tubules was found in the single-dose group (0.70 mmol/kg). These changes were no longer evident on day 15. For the dogs in the repeat-dose groups, there was reversible renal tubule degeneration in both sexes for medium dose (0.21 mmol/kg/d) and high dose (0.70 mmol/kg/d). No renal abnormality was found in the dogs that received repeated low doses (0.07 mmol/kg/d). The NOAEL of MT218 was 1.39 mmol/kg after a single dose and 0.46 mmol/kg/d after repeated dose in SD rats for 14 days. The NOAEL was considered to be 0.07 mmol/kg/d after repeated dose for 14 days in dogs. The toxicity study revealed that the dog is the more sensitive species.

After daily IV administration for 14 consecutive days, systemic exposure ($AUC_{0–24h}$ and C_0) of MT218 in SD rat plasma increased as the dose increased on D1 and D14, and there was no substantial sex difference. The accumulation ratios, $AUC_{0–24h}$ (D14)/$AUC_{0–24h}$ (D1), of Gd for the low, medium, and high dose on day 14 were 1.52, 1.49, and 1.31 for male rats and 1.41, 1.61, and 1.22 for female rats, respectively. For dogs, accumulation ratios, $AUC_{0–24h}$ (D14)/$AUC_{0–24h}$ (D1), of Gd for the low, medium, and high dose on days 1 and 14 were 0.92, 1.07, and 1.02 for male dogs and 0.91, 0.99, and 1.00 for female dogs, respectively. Thus, a minimal accumulation was observed in rats and dogs.

Gd level in rat tissues was determined after euthanization of the rats on day 15 after receiving a single dose and on day 29 in the repeated-dose groups. In the group that received a single dose of 1.39 mmol/kg, the highest Gd concentration was found in the kidneys of the rats, whereas other tissues exhibited lower Gd concentrations (<1/20 of the kidney concentration). Gd was not detected in the brain and muscles. For the 3 repeated-dose groups, Gd tissue concentrations on day 29 were similar to those of the single-dose group on day 15. The Gd tissue concentration on day 29 is shown in Table 5.

TABLE 5. Concentrations of Gd in Rat Tissues on Day 29 (After the 2-Week Recovery Period)

Dose, mmol/kg/d	Tissue	Measured Concentration, μg/g Tissue			
		Male		Female	
		Mean	SD	Mean	SD
0.15	Bone	0.28	0.15	0.19	0.12
	Brain	BQL	NA	BQL	NA
	Colon	0.18	0.06	0.15	0.09
	Heart	0.14	0.13	BQL	NA
	Jejunum	0.17	0.11	0.23	0.12
	Kidney	15.15	8.97	26.46	8.22
	Liver	0.22	0.05	0.31	0.17
	Lung	BQL	NA	0.20	0.04
	Muscle	BQL	NA	0.03	0.07
	Skin	0.13	0.03	0.14	0.02
	Spleen	0.37	0.08	0.32	0.22
0.46	Bone	0.70	0.71	1.13	0.99
	Brain	0.07	0.08	0.03	0.06
	Colon	0.79	0.23	1.02	0.10
	Heart	1.72	NA	3.17	3.63
	Jejunum	0.73	0.26	0.73	0.23
	Kidney	70.70	22.04	100.81	34.15
	Liver	1.96	2.42	1.03	0.26
	Lung	1.33	0.18	1.27	NA
	Muscle	0.22	0.10	0.21	0.06
	Skin	0.95	0.47	1.26	0.35
	Spleen	1.12	0.25	1.41	0.29
1.39	Bone	5.85	2.27	4.90	4.30
	Brain	1.81	2.28	0.40	0.28
	Colon	3.92	0.89	3.44	0.71
	Heart	2.56	0.64	1.85	0.57
	Jejunum	3.72	1.15	3.26	1.35
	Kidney	519.85	230.47	346.00	222.23
	Liver	4.85	1.23	4.11	1.52
	Lung	4.83	3.03	3.86	1.58
	Muscle	1.15	0.57	1.27	0.60
	Skin	2.31	0.41	4.56	2.90
	Spleen	6.04	1.30	4.69	0.77

Gd indicates gadolinium; BQL, below limit of quantitation; NA, not available.

Genotoxicity

No positive mutagenic response with MT218 was observed at dose levels of 15, 50, 150, 500, 1500, and 5000 μg/plate in any testing strains (ie, TA97a, TA98, TA100, TA102, and TA1535 strains of *S. typhimurium*), either in the presence or absence of S9 activation. No significant changes in chromosomal aberration ratios were observed in CHL fibroblasts as compared with the control group ($P > 0.05$) at MT218 concentrations of 2000, 1000, and 500 μg/mL after 4 hours of treatment either with or without metabolic activation or after treatment for 27 hours without metabolic activation. In MT218-treated ICR mice, there was no significant decrease ($P > 0.05$) in the ratio of polychromatic erythrocytes to total erythrocytes in the low-, mid-, and high-dose MT218 groups or positive control group, indicating no bone marrow toxicity. In comparison with the vehicle control group, there was no significant increase in the incidence of micronuclei in the MT218 groups, indicating no genotoxicity of MT218 to bone marrow when administered at dose levels of 1.39, 0.70, and 0.35 mmol/kg/d for 2 days.

Other Toxicology Studies

MT218 injection had no hemolytic or aggregative effect at a concentration of 0.2 M in the hemolysis test with RBCs of New Zealand rabbits. The anaphylactic reaction was negative in guinea pigs when MT218 was dosed via intraperitoneal injection for sensitization at 0.200 or 0.695 mmol/kg, once every other day for 3 total doses, and then challenged by IV injection at 14 days and 21 days after the last sensitization using dosages of 0.40 and 1.39 mmol/kg.

DISCUSSION

In this work, we have characterized the physicochemical properties, metabolism, dosing effects, and imaging effectiveness at low doses for MRMI in different tumor models, as well as pharmacokinetics, tissue retention, and safety of MT218 in preparation for clinical translation.

MT218 possesses high r_1 relaxivities at 1.4 and 3.0 T, which encompass the most commonly used magnetic field strength range for clinical MRI. It is a small molecule with a moderate binding affinity to the ECM oncoprotein, EDB-FN, which allows it to rapidly bind and penetrate into inner tumor tissue through reversible binding. As a result, MT218 produces robust T_1 contrast enhancement at substantially lower doses than the clinical GBCA throughout the EDB-FN-rich aggressive solid tumors for at least 30 minutes postinjection, which indicated a potential lower dose for clinical diagnostic MRI. The results are consistent with the previously reported results from different types of solid tumors.[17,29–31,41]

MT218 shows chelating stability at physiological pH and only minor dissociation was observed exclusively at acidic pH and the presence of chelating agents, results similar to those of gadoteridol.[6,43] The peptide in the contrast agent is susceptible to enzymatic degradation in the blood plasma. It degrades faster in rat plasma than in human plasma, slower in dog plasma. Nevertheless, the plasma degradation of the agent does not prevent rapid EDB-FN-specific tumor accumulation sufficient to demonstrate MRI contrast enhancement. Robust enhancement is still observed in the rat PC3 tumor model for at least 30 minutes at both 0.04 and 0.02 mmol/kg after IV injection. MT218 is also subject to metabolism by hepatocytes owing to enzymatic degradation of the peptide. It does not show any notable inhibitory, inductive, or other pharmacologic activities with the commonly tested protein targets.

Rapid excretion and complete clearance of MRI contrast agents after diagnostic imaging are essential for their safe clinical use, especially considering the potential toxic side effects related to prolonged Gd tissue retention.[44,45] The preclinical assessment has shown that MT218 possesses pharmacokinetics, excretion, and tissue retention similar to gadoteridol, one of the safest macrocyclic GBCAs, and other clinical macrocyclic GBCAs.[46] Greater than 80% of the injected dose is excreted in urine within the first 8 hours postinjection in rats after a single dose. The biodistribution study in rats revealed that the Gd concentration decreased to 1.0 μg/g or lower in the tested tissues besides the kidneys, the organ that the agent is mainly excreted through, and fell to undetectable limits by 48 hours in most tissues. The distribution and clearance of MT218 in the kidneys were comparable to other clinical macrocyclic GBCAs, including gadoteridol, gadobutrol and gadoterate. Notably, MT218 brain levels were lowest among tissues tested, even with daily dosing for 2 weeks, similar to the results of the clinical macrocyclic GBCAs.[47–49] There is thus every expectation for the results in human studies to mirror those of the clinical macrocyclic GBCAs in regard to Gd retention in brain, namely, insignificance.

Studies on GLP toxicity have shown that MT218 exhibits low toxicity in rats and dogs after single and repeated dosing at relatively high doses. Dose-related renal effects are observed after repeated daily administrations for 14 days. However, such effects have also been observed for other clinical GBCAs.[50–53] The NOAEL from the most sensitive preclinical species (dog) was not established for single dosing and was 0.07 mmol/kg/d for repeated daily IV dosing. The targeted contrast agent is expected to be used clinically as a single dose for diagnostic MRI at 0.04 mmol/kg or lower based on the preclinical efficacy in multiple mouse and rat xenograft tumor models, lower than its repeated dosing NOAEL in dogs. Overall, the preclinical studies have shown that MT218 possesses an excellent safety profile for advancing to clinical evaluations.

Nephrogenic systemic fibrosis and brain Gd deposition related to the prolonged retention of GBCAs have raised safety concerns of their clinical use. In 2014, Kanda et al[54] reported elevated signal in the deep brain of patients with normal renal status who had experienced multiple doses (eg, 5–6) of linear GBCA. Many studies have been performed since, and most reported that (1) the elevated signal correlates with linear versus macrocyclic GBCA, mirroring the trend as observed in nephrogenic systemic fibrosis patients[55]; (2) the trends were replicated in rodents, that Gd concentration measured by an absolute method (ICP-MS) is indeed correlated with MRI signal and geographically as determined in human cadavers that had had multiple GBCA doses in life[49]; and (3) no neurologic toxicity nor symptomology has been recorded in cadavers or living patients that was associated with these Gd retention findings, even for the linear GBCA.[56] The elevated signal that GBCA imparts to tissues generally requires a minimum, micromolar Gd concentration to visualize signal elevation in MRI. Linear GBCAs are well known to deliver much greater free Gd released from GBCA injections, which is retained longer and hence accumulates in bones, skin, and even in brain when multiple doses are administered. MT218 uses the macrocyclic gadoteridol chelate, having the lowest Gd retention in experimental rodents among the GBCA, and a single dose of MT218 is prescribed in phase 1 clinical trial. Notably, an animal biodistribution study of MT218 revealed no observed brain retention in rats in single- and repeated-dose studies where the LLOQ was 0.1 ppm. However, the contraindication for use among the most vulnerable patients with renal dysfunction is yet to be determined for MT218 in later-phase clinical studies. To protect subjects from this risk, subjects with signs of impaired renal function are always excluded for GBCA in early-phase clinical studies.

The success of this tumor-targeting MRI contrast agent in safety and efficacy will shed light on other products of the same series and imaging agents aiming at the ECM, whose content is known to be related to tumor aggressiveness. A number of preclinical attempts have been published that sought to use MRI to image malignant tumors using GBCA targeted to fibrin or FN.[8,12,57–60] The target for these agents has sufficient Gd concentration to produce MRI signal with reasonable injected doses. The primary negative issue with these agents is the target itself (fibrin or untransformed FN), however, which is commonly distributed in non-tumor tissue. The target of MT218, EDB-FN retains a high concentration of fibrin/FN but is highly and specifically expressed only in aggressive malignancies, with little expression in normal tissues. Based on the preclinical investigations, MT218 has the potential to be used for early detection of multiple types of EDB-FN-rich aggressive solid tumors, including breast cancer, colon cancer, lung cancer, pancreatic cancer, prostate cancer, and others with high-resolution MRMI. Because EDB-FN expression is associated with invasiveness of cancer cells, MRMI of EDB-FN also has the potential for noninvasive characterization of aggressive tumors and monitoring disease progression and therapeutic response based on the EDB-FN expression levels.

This study was focused on the preclinical assessments of a peptide-targeted, small molecular GBCA for specific cancer MRI in clinical translation. The dose-dependent efficacy of MT218 for specific contrast enhancement of aggressive tumors was evaluated in tumor xenografts or allografts in rodents. The pharmacokinetics, biodistribution, and safety of the agent were investigated in a small number of animals of 2 species, including rats and dogs. The clinical studies are needed to demonstrate the pharmacokinetics, safety, and specific cancer MRI of MT218 in patients for clinical development. Currently, an investigative new drug application was approved by the FDA. A phase 1 clinical trial for safety assessments of MT218 is ongoing in healthy volunteers. The efficacy of MT218 in MRI of aggressive tumors will be evaluated in late-phase clinical trials once its safety is demonstrated in humans.

In conclusion, our study results demonstrate that the small molecular peptide targeted MRI contrast agent MT218 has a high r_1 relaxivity and produces robust contrast enhancement in EDB-FN-rich tumors in rodents at low doses. It shows chelating stability comparable with the base clinical macrocyclic contrast agent. The pharmacokinetics, excretion, and biodistribution data in animals indicate that MT218 behaves similarly to the clinical macrocyclic GBCAs with rapid clearance and minimal tissue retention, especially with no detectable long-term retention in the brain. The results of in vitro and in vivo safety and pharmacology studies demonstrate a satisfactory safety profile that warrants further clinical evaluations of the targeted contrast agent for cancer MRI.

ACKNOWLEDGMENTS

This work was supported in part by the National Institutes of Health grants R44 CA199826 and R01 CA211762, and Jiansu Ronghui Motek Pharmaceuticals, Inc.

REFERENCES

1. Biswas J, Nelson CB, Runge VM, et al. Brain tumor enhancement in magnetic resonance imaging: comparison of signal-to-noise ratio (SNR) and contrast-to-noise ratio (CNR) at 1.5 versus 3 tesla. *Invest Radiol*. 2005;40:792–797.
2. Yuh WT, Mayr NA, Jarjoura D, et al. Predicting control of primary tumor and survival by DCE MRI during early therapy in cervical cancer. *Invest Radiol*. 2009;44: 343–350.
3. Tosun M, Uslu H. Prebiopsy multiparametric MRI and PI-RADS version 2.0 for differentiating histologically benign prostate disease from prostate cancer in biopsies: a retrospective single-center comparison. *Clin Imaging*. 2021;78:98–103.
4. Maggi M, Del Giudice F, Falagario UG, et al. SelectMDx and multiparametric magnetic resonance imaging of the prostate for men undergoing primary prostate biopsy: a prospective assessment in a multi-institutional study. *Cancers (Basel)*. 2021;13:2047.
5. Unger EC, Totty WG, Neufeld DM, et al. Magnetic resonance imaging using gadolinium labeled monoclonal antibody. *Invest Radiol*. 1985;20:693–700.
6. Overoye-Chan K, Koerner S, Looby RJ, et al. EP-2104R: a fibrin-specific gadolinium-based MRI contrast agent for detection of thrombus. *J Am Chem Soc*. 2008;130: 6025–6039.
7. Ferrauto G, Tripepi M, Di Gregorio E, et al. Detection of U-87 tumor cells by RGD-functionalized/Gd-containing giant unilamellar vesicles in magnetization transfer contrast magnetic resonance images. *Invest Radiol*. 2021;56:301–312.
8. Atanasova I, Sojoodi M, Leitão HS, et al. Molecular magnetic resonance imaging of fibrin deposition in the liver as an Indicator of tissue injury and inflammation. *Invest Radiol*. 2020;55:209–216.
9. Shuvaev S, Akam E, Caravan P. Molecular MR contrast agents. *Invest Radiol*. 2021;56:20–34.
10. Sipkins DA, Cheresh DA, Kazemi MR, et al. Detection of tumor angiogenesis in vivo by alphaVbeta3-targeted magnetic resonance imaging. *Nat Med*. 1998;4: 623–626.
11. Boyd AS, Zic JA, Abraham JL. Gadolinium deposition in nephrogenic fibrosing dermopathy. *J Am Acad Dermatol*. 2007;56:27–30.
12. Ye F, Wu X, Jeong EK, et al. A peptide targeted contrast agent specific to fibrin-fibronectin complexes for cancer molecular imaging with MRI. *Bioconjug Chem*. 2008;19:2300–2303.
13. Ebbinghaus C, Scheuermann J, Neri D, et al. Diagnostic and therapeutic applications of recombinant antibodies: targeting the extra-domain B of fibronectin, a marker of tumor angiogenesis. *Curr Pharm Des*. 2004;10:1537–1549.
14. Han Z, Lu ZR. Targeting fibronectin for cancer imaging and therapy. *J Mater Chem B*. 2017;5:639–654.
15. Gao D, Vahdat LT, Wong S, et al. Microenvironmental regulation of epithelial-mesenchymal transitions in cancer. *Cancer Res*. 2012;72:4883–4889.
16. Vaidya A, Wang H, Qian V, et al. Overexpression of extradomain-B fibronectin is associated with invasion of breast cancer cells. *Cells*. 2020;9:1826.
17. Vaidya A, Ayat N, Buford M, et al. Noninvasive assessment and therapeutic monitoring of drug-resistant colorectal cancer by MR molecular imaging of extradomain-B fibronectin. *Theranostics*. 2020;10:11127–11143.
18. Petrini I, Barachini S, Carnicelli V, et al. ED-B fibronectin expression is a marker of epithelial-mesenchymal transition in translational oncology. *Oncotarget*. 2017; 8:4914–4921.
19. Kaspar M, Zardi L, Neri D. Fibronectin as target for tumor therapy. *Int J Cancer*. 2006;118:1331–1339.
20. Inufusa H, Nakamura M, Adachi T, et al. Localization of oncofetal and normal fibronectin in colorectal cancer. Correlation with histologic grade, liver metastasis, and prognosis. *Cancer*. 1995;75:2802–2808.
21. Menzin AW, Loret de Mola JR, Bilker WB, et al. Identification of oncofetal fibronectin in patients with advanced epithelial ovarian cancer: detection in ascitic fluid and localization to primary sites and metastatic implants. *Cancer*. 1998;82: 152–158.
22. Tijink BM, Perk LR, Budde M, et al. (124)I-L19-SIP for immuno-PET imaging of tumour vasculature and guidance of (131)I-L19-SIP radioimmunotherapy. *Eur J Nucl Med Mol Imaging*. 2009;36:1235–1244.
23. Jailkhani N, Ingram JR, Rashidian M, et al. Noninvasive imaging of tumor progression, metastasis, and fibrosis using a nanobody targeting the extracellular matrix. *Proc Natl Acad Sci U S A*. 2019;116:14181–14190.
24. Sun Y, Kim HS, Park J, et al. MRI of breast tumor initiating cells using the extra domain-B of fibronectin targeting nanoparticles. *Theranostics*. 2014;4:845–857.
25. Han Z, Zhou Z, Shi X, et al. EDB fibronectin specific peptide for prostate cancer targeting. *Bioconjug Chem*. 2015;26:830–838.
26. Han Z, Li Y, Roelle S, et al. Targeted contrast agent specific to an Oncoprotein in tumor microenvironment with the potential for detection and risk stratification of prostate cancer with MRI. *Bioconjug Chem*. 2017;28:1031–1040.
27. Han Z, Cheng H, Parvani JG, et al. Magnetic resonance molecular imaging of metastatic breast cancer by targeting extradomain-B fibronectin in the tumor microenvironment. *Magn Reson Med*. 2018;79:3135–3143.
28. Ayat NR, Qin JC, Cheng H, et al. Optimization of ZD2 peptide targeted Gd(HP-DO3A) for detection and risk-stratification of prostate cancer with MRI. *ACS Med Chem Lett*. 2018;9:730–735.
29. Hall RC, Ayat NR, Qiao PL, et al. Preclinical assessment of the effectiveness of magnetic resonance molecular imaging of extradomain-B fibronectin for detection and characterization of oral cancer. *Mol Imaging Biol*. 2020;22:1532–1542.
30. Qiao P, Ayat NR, Vaidya A, et al. Magnetic resonance molecular imaging of extradomain B fibronectin improves imaging of pancreatic Cancer tumor xenografts. *Front Oncol*. 2020;10:586727.
31. Ayat NR, Vaidya A, Yeung GA, et al. Effective MR molecular imaging of triple negative breast cancer with an EDB-fibronectin-specific contrast agent at reduced doses. *Front Oncol*. 2019;9:1351.
32. Schilb AL, Ayat NR, Vaidya AM, et al. Efficacy of targeted ECO/miR-200c nanoparticles for modulating tumor microenvironment and treating triple negative breast cancer as non-invasively monitored by MR molecular imaging. *Pharm Res*. 2021;38:1405–1418.
33. Dahlin JL, Nelson KM, Strasser JM, et al. Assay interference and off-target liabilities of reported histone acetyltransferase inhibitors. *Nat Commun*. 2017;8:1527.
34. White GW, Gibby WA, Tweedle MF. Comparison of Gd(DTPA-BMA) (Omniscan) versus Gd(HP-DO3A) (ProHance) relative to gadolinium retention in human bone tissue by inductively coupled plasma mass spectroscopy. *Invest Radiol*. 2006;41: 272–278.
35. Müller L, Kikuchi Y, Probst G, et al. ICH-harmonised guidances on genotoxicity testing of pharmaceuticals: evolution, reasoning and impact. *Mutat Res*. 1999; 436:195–225.
36. Laurent S, Elst LV, Muller RN. Comparative study of the physicochemical properties of six clinical low molecular weight gadolinium contrast agents. *Contrast Media Mol Imaging*. 2006;1:128–137.
37. Rohrer M, et al. Comparison of magnetic properties of MRI contrast media solutions at different magnetic field strengths. *Invest Radiol*. 2005;40:715–724.
38. Dumas S, Jacques V, Sun WC, et al. High relaxivity magnetic resonance imaging contrast agents, part 1: impact of single donor atom substitution on relaxivity of serum albumin-bound gadolinium complexes. *Invest Radiol*. 2010;45:600–612.
39. Jacques V, Dumas S, Sun WC, et al. High-relaxivity magnetic resonance imaging contrast agents, part 2: optimization of inner- and second-sphere relaxivity. *Invest Radiol*. 2010;45:613–624.
40. Vymazal J, Bauer H, Mintorovitch J, et al. Thrombus imaging with fibrin-specific gadolinium-based MR contrast agent EP-2104R: results of a phase II clinical study of feasibility. *Invest Radiol*. 2009;44:697–704.
41. Qiao PL, Gargesha M, Liu Y, et al. Magnetic resonance molecular imaging of extradomain B fibronectin enables detection of pancreatic ductal adenocarcinoma metastasis. *Magn Reson Imaging*. 2022;86:37–45.
42. Eakins MN, Eaton SM, Fisco RA, et al. Physicochemical properties, pharmacokinetics, and biodistribution of gadoteridol injection in rats and dogs. *Acad Radiol*. 1995;2:584–591.
43. Kumar K, Chang CA, Tweedle MF. Equilibrium and kinetic studies of lanthanide complexes of macrocyclic polyamino carboxylates. *Inorg Chem*. 1993;1993: 587–593.
44. Zhou IY, Ramsay IA, Ay I, et al. Positron emission tomography-magnetic resonance imaging pharmacokinetics, in vivo biodistribution, and whole-body elimination of Mn-PyC3A. *Invest Radiol*. 2021;56:261–270.
45. Lancelot E. Revisiting the pharmacokinetic profiles of gadolinium-based contrast agents: differences in long-term biodistribution and excretion. *Invest Radiol*. 2016;51:691–700.
46. Tweedle MF, Wedeking P, Kumar K. Biodistribution of radiolabeled, formulated gadopentetate, gadoteridol, gadoterate, and gadodiamide in mice and rats. *Invest Radiol*. 1995;30:372–380.
47. Jost G, Frenzel T, Boyken J, et al. Long-term excretion of gadolinium-based contrast agents: linear versus macrocyclic agents in an experimental rat model. *Radiology*. 2019;290:340–348.
48. Tweedle MF. Gadolinium retention in human brain, bone, and skin. *Radiology*. 2021;300:570–571.
49. Lohrke J, Frisk AL, Frenzel T, et al. Histology and gadolinium distribution in the rodent brain after the administration of cumulative high doses of linear and macrocyclic gadolinium-based contrast agents. *Invest Radiol*. 2017;52:324–333.
50. Aime S, Caravan P. Biodistribution of gadolinium-based contrast agents, including gadolinium deposition. *J Magn Reson Imaging*. 2009;30:1259–1267.
51. Rogosnitzky M, Branch S. Gadolinium-based contrast agent toxicity: a review of known and proposed mechanisms. *Biometals*. 2016;29:365–376.

52. Elmståhl B, Nyman U, Leander P, et al. Gadolinium contrast media are more nephrotoxic than iodine media. The importance of osmolality in direct renal artery injections. *Eur Radiol*. 2006;16:2712–2720.

53. Akgun H, Gonlusen G, Cartwright J Jr., et al. Are gadolinium-based contrast media nephrotoxic? A renal biopsy study. *Arch Pathol Lab Med*. 2006;130:1354–1357.

54. Kanda T, Fukusato T, Matsuda M, et al. Gadolinium-based contrast agent accumulates in the brain even in subjects without severe renal dysfunction: evaluation of autopsy brain specimens with inductively coupled plasma mass spectroscopy. *Radiology*. 2015;276:228–232.

55. Boyken J, Frenzel T, Lohrke J, et al. Gadolinium accumulation in the deep cerebellar nuclei and globus pallidus after exposure to linear but not macrocyclic gadolinium-based contrast agents in a retrospective pig study with high similarity to clinical conditions. *Invest Radiol*. 2018;53:278–285.

56. Layne KA, Raja K, Dargan PI, et al. Gadolinium concentrations in biological matrices from patients exposed to gadolinium-based contrast agents. *Invest Radiol*. 2021;56:458–464.

57. Spuentrup E, et al. Molecular magnetic resonance imaging of coronary thrombosis and pulmonary emboli with a novel fibrin-targeted contrast agent. *Circulation*. 2005;111:1377–1382.

58. Morelli JN, Runge VM, Williams JM, et al. Evaluation of a fibrin-binding gadolinium chelate peptide tetramer in a brain glioma model. *Invest Radiol*. 2011;46:169–177.

59. Uppal R, Medarova Z, Farrar CT, et al. Molecular imaging of fibrin in a breast cancer xenograft mouse model. *Invest Radiol*. 2012;47:553–558.

60. Tan M, Ye Z, Jeong EK, et al. Synthesis and evaluation of nanoglobular macrocyclic Mn(II) chelate conjugates as non-gadolinium(III) MRI contrast agents. *Bioconjug Chem*. 2011;22:931–937.